LEVEL

DAVID W. TAYLOR NAVAL SHIP
RESEARCH AND DEVELOPMENT CENTER

Bethesda, Md. 20084

AERODYNAMIC CHARACTERISTICS OF THE CLOSE-COUPLED CANARD
AS APPLIED TO LOW-TO-MODERATE SWEPT WINGS
VOLUME 1. GENERAL TRENDS

by

David W. Lacey

Final rept. 1974-1977.

APPROVED FOR PUBLIC RELEASE: DISTRIBUTION UNLIMITED

D D C

JAN 29 1979

A

AVIATION AND SURFACE EFFECTS DEPARTMENT
RESEARCH AND DEVELOPMENT REPORT

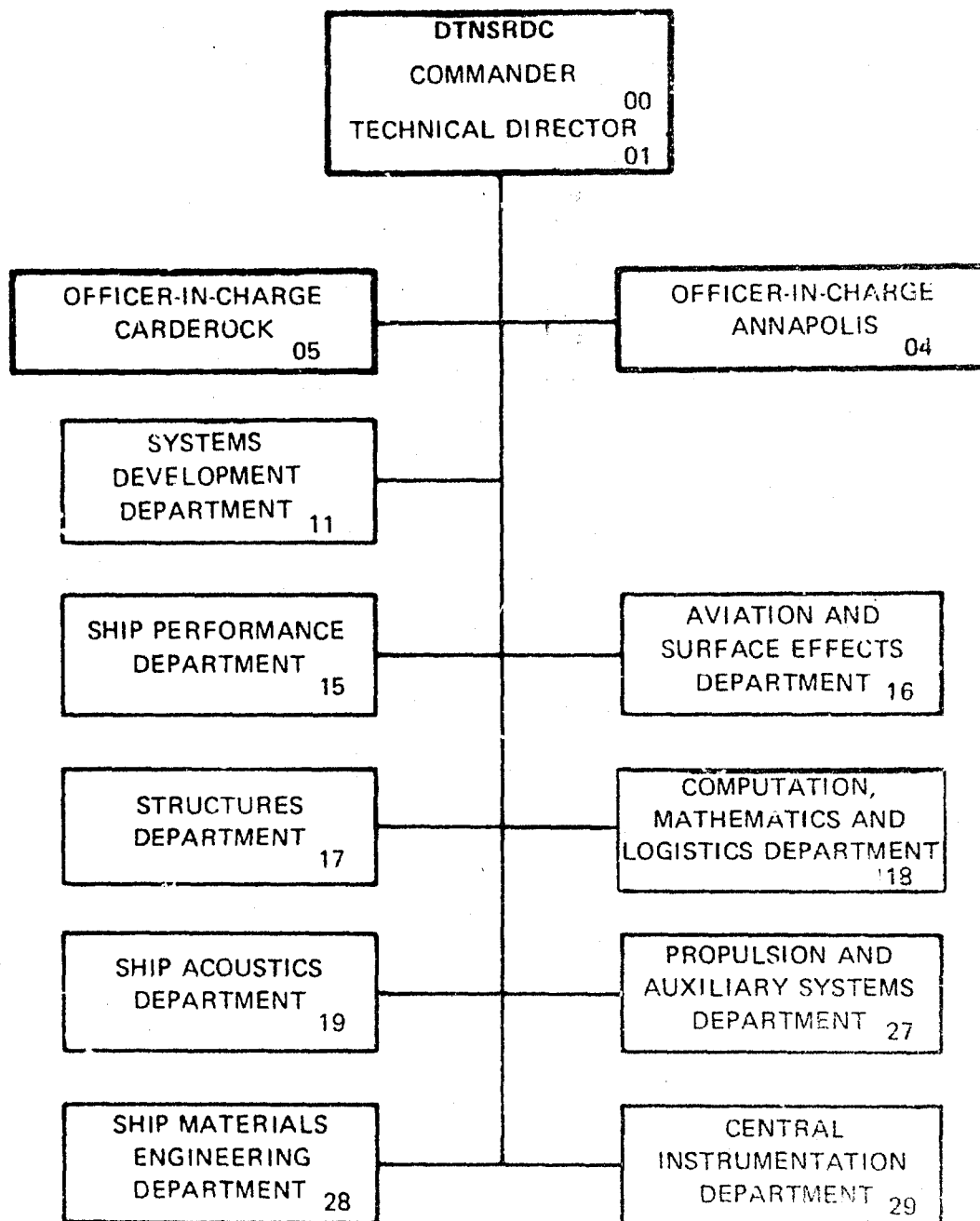F14142   WF14142109

Jan 1979   68 p.   DTNSRDC 79/001-

AERO-1256-

MAJOR DTNSRDC ORGANIZATIONAL COMPONENTS

```
                    ┌─────────────────────────┐
                    │       DTNSRDC           │
                    │      COMMANDER          │
                    │                    00   │
                    │ TECHNICAL DIRECTOR      │
                    │                    01   │
                    └─────────────────────────┘
```

OFFICER-IN-CHARGE CARDEROCK 05	OFFICER-IN-CHARGE ANNAPOLIS 04
SYSTEMS DEVELOPMENT DEPARTMENT 11	
SHIP PERFORMANCE DEPARTMENT 15	AVIATION AND SURFACE EFFECTS DEPARTMENT 16
STRUCTURES DEPARTMENT 17	COMPUTATION, MATHEMATICS AND LOGISTICS DEPARTMENT 18
SHIP ACOUSTICS DEPARTMENT 19	PROPULSION AND AUXILIARY SYSTEMS DEPARTMENT 27
SHIP MATERIALS ENGINEERING DEPARTMENT 28	CENTRAL INSTRUMENTATION DEPARTMENT 29

REPORT DOCUMENTATION PAGE		READ INSTRUCTIONS BEFORE COMPLETING FORM
1. REPORT NUMBER DTNSRDC-79/001	2. GOVT ACCESSION NO.	3. RECIPIENT'S CATALOG NUMBER
4. TITLE (and Subtitle) AERODYNAMIC CHARACTERISTICS OF THE CLOSE-COUPLED CANARD AS APPLIED TO LOW-TO-MODERATE SWEPT WINGS VOLUME 1: GENERAL TRENDS		5. TYPE OF REPORT & PERIOD COVERED Final
		6. PERFORMING ORG. REPORT NUMBER Aero Report 1256
7. AUTHOR(s) David W. Lacey		8. CONTRACT OR GRANT NUMBER(s)
9. PERFORMING ORGANIZATION NAME AND ADDRESS David W. Taylor Naval Ship Research and Development Center Bethesda, Maryland 20084		10. PROGRAM ELEMENT, PROJECT, TASK AREA & WORK UNIT NUMBERS Program Element 62241N Task Area WF 1-41421-09 Work Unit 1600-078
11. CONTROLLING OFFICE NAME AND ADDRESS Naval Air Systems Command AIR 320 Washington, D.C. 20361		12. REPORT DATE January 1979
		13. NUMBER OF PAGES 67
14. MONITORING AGENCY NAME & ADDRESS(if different from Controlling Office)		15. SECURITY CLASS. (of this report) UNCLASSIFIED
		15a. DECLASSIFICATION/DOWNGRADING SCHEDULE

16. DISTRIBUTION STATEMENT (of this Report)

APPROVED FOR PUBLIC RELEASE: DISTRIBUTION UNLIMITED

17. DISTRIBUTION STATEMENT (of the abstract entered in Block 20, if different from Report)

18. SUPPLEMENTARY NOTES

19. KEY WORDS (Continue on reverse side if necessary and identify by block number)

Close-Coupled Canards   Interference
Lift   Deflection
Drag
Pitching Moment

20. ABSTRACT (Continue on reverse side if necessary and identify by block number)

A summary of the general findings of close-coupled canard research at David W. Taylor Naval Ship Research and Development Center is presented. These findings are based on a series of wind-tunnel evaluations utilizing an aircraft research model having wings of either 25- or 50-degree leading edge sweep.

Best Available Copy

(Continued on reverse side)

DD FORM 1473 EDITION OF 1 NOV 65 IS OBSOLETE
S/N 0102-LF-014-6601

(Block 20 continued)

Discussed is the effect of canard placement on lift, drag, and pitching moment and the location of optimum position for canards of different planform. In addition, the effects of canard-wing interference, canard deflection, size, and Mach number are described.

FOREWORD

This report summarizes the findings of close-coupled canard research performed by the Aviation and Surface Effects Department of the David W. Taylor Naval Ship Research and Development Center. The work was performed between 1970 and 1974 and was funded by the Naval Air Systems Command (AIR 320). The purpose of the report is to provide a summary of the aerodynamic findings obtained from a series of wind-tunnel evaluations involving three general research models and the F-4 aircraft. The report is presented in four volumes: Volume 1: General Trends; Volume 2: Subsonic Speed Regime; Volume 3: Transonic-Supersonic Speed Regime; and Volume 4: F-4 Phantom II Aircraft.

TABLE OF CONTENTS

LIST OF FIGURES

LIST OF TABLES

AR	Aspect Ratio
C_D	Drag coefficient, drag/qS_w
C_{D_B}	Drag coefficient of body alone
$C_{D_{B+C}}$	Drag coefficient of body plus canard
$C_{D_{B+H}}$	Drag coefficient of body plus horizontal tail
$C_{D_{WB}}$	Drag coefficient of body plus wing
C_{D_0}	Drag coefficient evaluated at zero lift
C_i	Canard
C_L	Lift coefficient, lift/qS_w
C_{L_B}	Lift coefficient of body alone
$C_{L_{B+C}}$	Lift coefficient of body plus canard
$C_{L_{B+H}}$	Lift coefficient of body plus horizontal tail
$C_{L_{max}}$	Maximum lift coefficient
$C_{L_{WB}}$	Lift coefficient of body plus wing
$C_{L_{20}}$	Lift coefficient evaluated at 20-degrees angle of attack
C_{L_α}	Lift curve slope, $\partial C_L / \partial \alpha$
C_M	Pitching moment coefficient, pitching moment/$qS_w \bar{c}$

C_{M_B}	Pitching moment coefficient of body alone
$C_{M_{B+C}}$	Pitching moment coefficient of body plus canard
$C_{M_{B+H}}$	Pitching moment coefficient of body plus horizontal tail
$C_{M_{WB}}$	Pitching moment coefficient of body plus wing
C_{N_C}	Canard normal force coefficient, normal force/qS
$\bar{c}$	Mean aerodynamic chord, inches
i	Canard shape
j	Canard position
$(L/D)_{max}$	Maximum lift-to-drag ratio
M	Mach number
P_j	Canard position
q	Dynamic pressure, pounds per square foot
S_C	Canard projected area, square feet
S_H	Horizontal tail projected area, square feet
S_W	Wing reference area, square feet
$\bar{x}$	Longitudinal distance, inches
$\bar{z}$	Vertical distance, inches
α	Angle of attack, degrees
ΔC_D	$C_D - C_{D_{WB}}$
ΔC_{D_C}	$C_{D_{B+C}} - C_{D_B}$

ΔC_{D_H} $\qquad$ $C_{D_{B+H}} - C_{D_B}$

ΔC_L $\qquad$ $C_L - C_{L_{WB}}$

ΔC_{L_C} $\qquad$ $C_{L_{B+C}} - C_{L_B}$

ΔC_{L_H} $\qquad$ $C_{L_{B+H}} - C_{L_B}$

ΔC_{L_5} $\qquad$ ΔC_L evaluated at 5-degrees angle of attack

ΔC_M $\qquad$ $C_M - C_{M_{WB}}$

ΔC_{M_C} $\qquad$ $C_{M_{B+C}} - C_{M_B}$

ΔC_{M_H} $\qquad$ $C_{M_{B+H}} - C_{M_B}$

ΔC_{M_5} $\qquad$ ΔC_M evaluated at 5-degrees angle of attack

δ_c $\qquad$ Deflection angle, degrees

ϕ $\qquad$ $\dfrac{\left(C_{L_{max}} * (L/D)_{max}\right) \text{ canard + body-wing}}{\left(C_{L_{max}} * (L/D)_{max}\right) \text{ body-wing}}$

x

ABSTRACT

A summary of the general findings of close-coupled
canard research at David W. Taylor Naval Ship Research
and Development Center is presented. These findings are
based on a series of wind-tunnel evaluations utilizing
an aircraft research model having wings of either 25- or
50-degree leading edge sweep.

Discussed is the effect of canard placement on lift,
drag, and pitching moment and the location of optimum
position for canards of different planform. In addition,
the effects of canard-wing interference, canard deflec-
tion, size, and Mach number are described.

ADMINISTRATIVE INFORMATION

INTRODUCTION

The Wright Brothers used a canard geometry on the first aircraft.
Since that time, however, there have been few attempts at utilizing canard
surfaces on manned aircraft. The few attempts that have been made were
generally used as control devices and suffered numerous problems, as in the
case of the Curtiss Ascender aircraft where stall problems of the wing and
canard were serious--even fatal. Missiles often had good success using
small canard surfaces utilized as control devices.

The first really successful operational use of the canard can be
credited to the SAAB AJ-37 Viggen aircraft. The canard utilized on the
Viggen is of a close-coupled canard as opposed to the missile type or long
canard. The respective location of the canard in each of these cases is
shown in Figure 1.

Reference 1* presents the philosophy and methodology utilized in the
basic design of the canard-wing system of the Viggen aircraft. The design
is based on the mutual interaction between the vortex systems of two highly

---

*A complete reference is given on page 55.
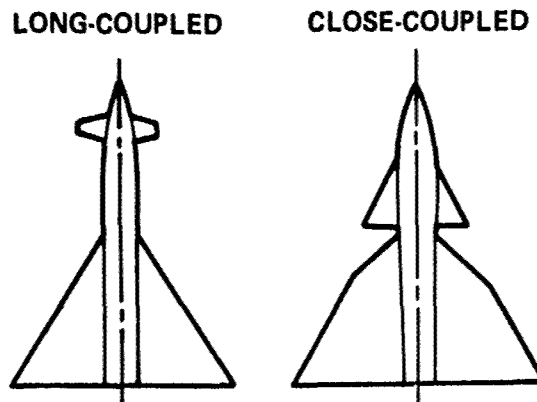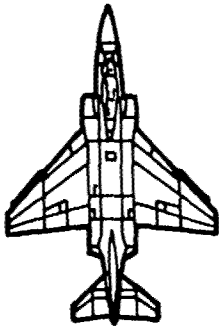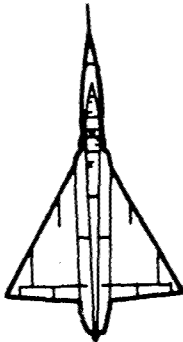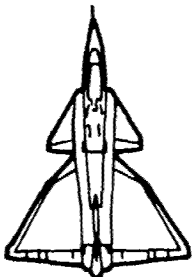
LONG-COUPLED   **CLOSE-COUPLED**

Figure 1 - Canard Geometry

swept delta wings in order to stabilize the vortices and thus develop high
lift coefficients for good short takeoff and landing (STOL) performance.
That the Viggen program did succeed in this goal is aptly demonstrated by
the values shown in Table 1. The table presents data for three aircraft:
(1) a conventional wing-tail aircraft, the F-4 Phantom II; (2) a pure
delta-wing aircraft, the F-106 Delta Dart; and (3) a close-coupled canard-
wing aircraft, the Viggen.

The Viggen has approximately 65 percent more lift coefficient (C_L) on
approach than the pure delta, although the wing loadings are approximately
the same. This gain in C_L results in a 34-knot reduction in approach
speed, thus assuring STOL capability. The gain in C_L is attributable to
the fact that the canard can generate a large lifting force and thus a large
nose-up moment which is trimmed out by positive wing elevon deflections.
Such trimming generates a positive trim lift increase. The pure delta,
however, must utilize negative elevon deflections which cause a lift loss.

For the Viggen to load the canard to high lift coefficients, it takes
advantage of the aforementioned vortex interactions. A sketch of these
interactions taken from a SAAB report is shown in Figure 2. The mutual
interactions allow the vortex systems to have greater stability and hence
higher lift than normal delta-wing configurations. Under these circum-
stances, the canard can lift to high values of canard normal force (C_N)
without occurring stall, as shown in Figure 3.

2

TABLE 1 – APPROACH CHARACTERISTICS OF F-4, F-106, AND VIGGEN AIRCRAFT

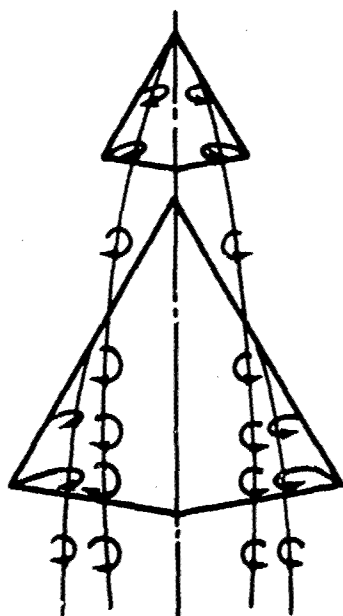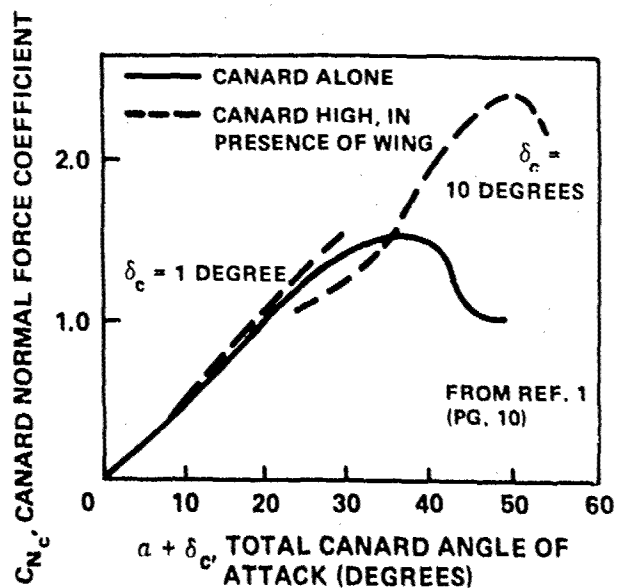|	McDONNELL DOUGLAS F-4 PHANTOM (U.S.)	GENERAL DYNAMICS/CONVAIR F-106 DELTA DART (U.S.)	SAAB-37 VIGGEN (SWEDEN)
WING LOADING, POUNDS PER SQUARE FOOT	64	39	40
APPROACH SPEED, KNOTS	134	153	119
APPROACH LIFT COEFFICIENT	1.04	0.49	0.84

Figure 2 – Vortex Interaction Patterns

Figure 3 – Effect of Wing-Canard Interaction on Canard Normal Force Coefficient

3

In order for this strong system of vorticies to occur, highly swept planforms are required ($\lambda \geq 60$). Navy aircraft, however, have almost exclusively been built with low-to-moderate swept wings ($\lambda \leq 50$). These low sweep angles have been dictated by the special requirements of carrier aviation such as aircraft size and approach speeds, as well as overall mission requirements such as range and/or endurance. Carrier approach speeds must be low, dictating either a high lift curve slope (C_{L_α}) or a light wing loading (W/S). However, light wing loading is detrimental to range and to overall aircraft size. Therefore, most Navy aircraft tend to have wing loadings in the range of $60 \leq W/S \leq 100$ pounds per square foot and low sweep angles in order to attain good lift characteristics and performance. The Viggen aircraft showed such significant promise that it was decided to investigate canard configurations further for use with wings having other than delta planform.
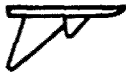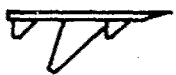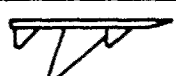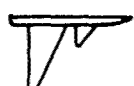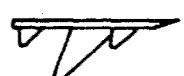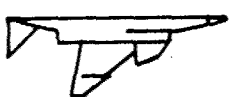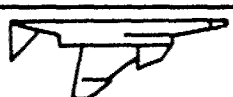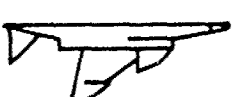
In order to accomplish this task, an extensive wind tunnel and analysis program was undertaken at the David W. Taylor Naval Ship Research and Development Center. The program began in 1970 and was completed in 1974. The initial program utilized a 50-degree swept wing research model with varying canard shapes, sizes, and positions. Later a 25-degree swept wing was utilized and many of the same canard parameters were repeated. Finally, a realistic aircraft configuration, the McDonnell F-4 Phantom II, was evaluated with a canard.

A listing of the various wind-tunnel evaluations and, where appropriate, the DTNSRDC report number are shown in Table 2.

The results of this series of wind-tunnel evaluations are discussed in this and the succeeding volumes. The first volume deals with general trends of close-coupled canards as applied to nondelta wings, including the effects of Mach number, wing sweep angle, interference effects between canard and wing, and canard placement, deflection, shape, and size. The second volume delineates, in more detail, the aforementioned parameters at subsonic speed. The third volume of this series deals with the canard in the transonic and supersonic speed regime. Included in this third volume is information on buffet. The fourth (final) volume is concerned with the

4

TABLE 2 - DTNSRDC CANARD WIND-TUNNEL PROGRAM

	Date	Tunnel	DTNSRDC ASED Report	Main Variable
	Jun 1970	Subsonic	AL 199	Canard size, position, deflection
	Dec 1970	Subsonic	--	Wing L.E. and droop, comparison with horizontal tail
	Dec 1970	Transonic	AL 81	Canard position, deflection, comparison with horizontal tail
	May 1971	Subsonic	AL 253	Canard Position, deflection
	Jul 1971	Supersonic	--	Canard position, deflection, buffet
	Aug 1971	Subsonic	--	Build-up data, canard interference
	Sep 1971	Subsonic	AL 91	Canard shapes, flow visualization studies
	Sep 1971	Transonic	AL 87	Canard position, deflection, comparison with tail, buffet
	Nov 1971	Transonic	AL 88	Canard shape, position, deflection, buffet
	Mar 1972	Transonic	AL 293	Canard size, position, deflection, aileron efficiency
	Jan 1973	Subsonic	ASED 304	Double delta canard, flaps and slats
	Mar 1973	Transonic	AL 303	Double delta canard, simulated free-float, slats

5

feasibility of adapting the canard to an operational aircraft, the F-4, and describes the gains in performance, the effects of the canard on flaps and ailerons, and the characteristics of the canard when it is allowed to free-float.

The main thrust of the DTNSRDC program was to improve high angle-of-attack maneuvering performance without sacrificing low angle-of-attack cruise performance for low-to-moderate-swept-wing aircraft. This goal was successfully accomplished and has demonstrated that close-coupled canards are a viable option for future Navy aircraft. Additionally, it was demonstrated that the close-coupled canard is not limited to use with highly swept delta-wing aircraft but is adaptable to aircraft of lower wing sweep.

DISCUSSION

CANARD-WING COUPLING

The conventional aft-mounted horizontal tail must produce a negative lifting force to provide a stabilizing force. The canard, on the other hand, produces a positive lifting force (adding to the total vehicle lift) when providing a stabilizing force. Thus, a canard configuration has a higher maximum lift coefficient than the tail configuration. The amount of increase in $C_{L_{max}}$ is primarily a function of the canard-to-wing area ratio (S_c/S_w) and canard placement. Furthermore, it was shown that by proper positioning of the canard-wing system it is possible to attain total lift greater than the sum of the lift of the individual components. Examples of this are shown in Figure 4 where the percentage change in $C_{L_{max}}$ versus canard-wing area ratio also is shown. The data are based on various National Advisory Committee for Aeronautics (NACA) as well as DTNSRDC configurations. The NACA configurations included the supersonic bomber SST type aircraft, however, several general research models were also tested. The values in brackets are the distance ratio between the wing 0.25 mean aerodynamic chord, $\bar{c}$, and the 0.40 exposed root chord of the canard. As can be seen, moving the canard further forward causes a large change in
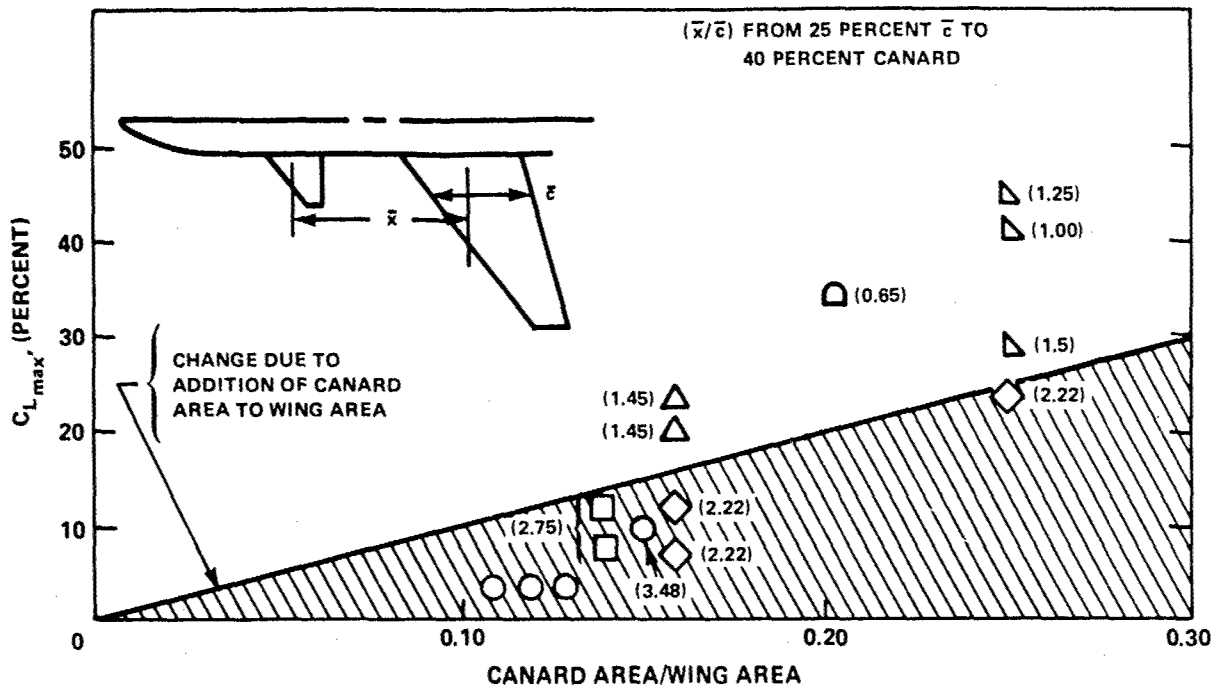
Figure 4 - Percent Change in Maximum Lift Coefficient
due to Canard

$C_{L_{max}}$ and, in fact, may reduce the value below that which could be obtained

merely by addition of the canard area to the wing area.

If the canard, however, is brought within 1.5 wing chords of the mean
aerodynamic chord (MAC), a different situation develops. Here, there is a
favorable interference between canard and wing and the maximum lift ob-
tained is greater than that which would occur due to the addition of the
canard area to the wing area. The following discussion will be concerned
with the range of $(\bar{x}/\bar{c})$ between approximately 0.5 to 1.5.

HIGH VERSUS LOW CANARD

It is possible to obtain a lower $C_{L_{max}}$ for the canard configuration
than for the wing alone depending on the vertical placement. In order to
obtain favorable interference, it is necessary to place the canard either
in the plane of the wing or above the wing plane. A comparison of the lift

7

and moment characteristics for a 45-degree truncated delta canard mounted above and below the wing chord plane is shown in Figure 5. The data were obtained at subsonic speeds as are the majority of the data presented in this volume. The canards are located approximately +0.2 $\bar{z}/\bar{c}$ above and below the wing chord plane. Two different canard deflections at 0 and +10 degrees are shown in Figure 6.

The model has a 50-degree swept wing having a 65A008 airfoil section swept back 25 degrees at the 0.27C line. The fuselage of the model is rectangular with rounded corners having a faired nose and boat tail. Dimensions of the model are given in the Appendix. The canard utilized a 45-degree truncated delta shape with a 64A008 airfoil section. The pivot point for the canard is located at the 40-percent point of the exposed root chord. The projected canard area is 20 percent of the wing area for the data presented in Figure 5. The canards are located at an $\bar{x}/\bar{c}$ of 1.25.

Examination of the data in Figure 5 reveals a lift increase relative to the configuration without a canard when the canard is located above the wing ("high") and no change in lift when the canard is located below the wing ("low") at zero-degree canard deflection. Deflection of the canard causes little change in lift for the canard above the wing but a lift loss at angles of attack above 12 degrees for the low canard.

Examination of the incremental pitching moment shown in Figure 7, reveals that the low canard is stalled at an angle of attack ($\alpha + \delta_c$, positive deflection) of approximately 15 degrees, whereas for the high canard there is no stall at least up to an $\alpha + \delta_c$ of 30 degrees. In fact, favorable interference occurs when the canard is located above and in close proximity to the wing.

CANARD VERSUS TAIL

Utilizing the same model as shown in Figure 6, typical canard-wing data are shown in Figure 8. Data are presented for both canard-wing, wing-horizontal tail, and wing alone. The canard is located at $\bar{x}/\bar{c}$ = 1.0 and $\bar{z}/\bar{c}$ = 0.2. The horizontal tail is of the same 45-degree truncated delta

8
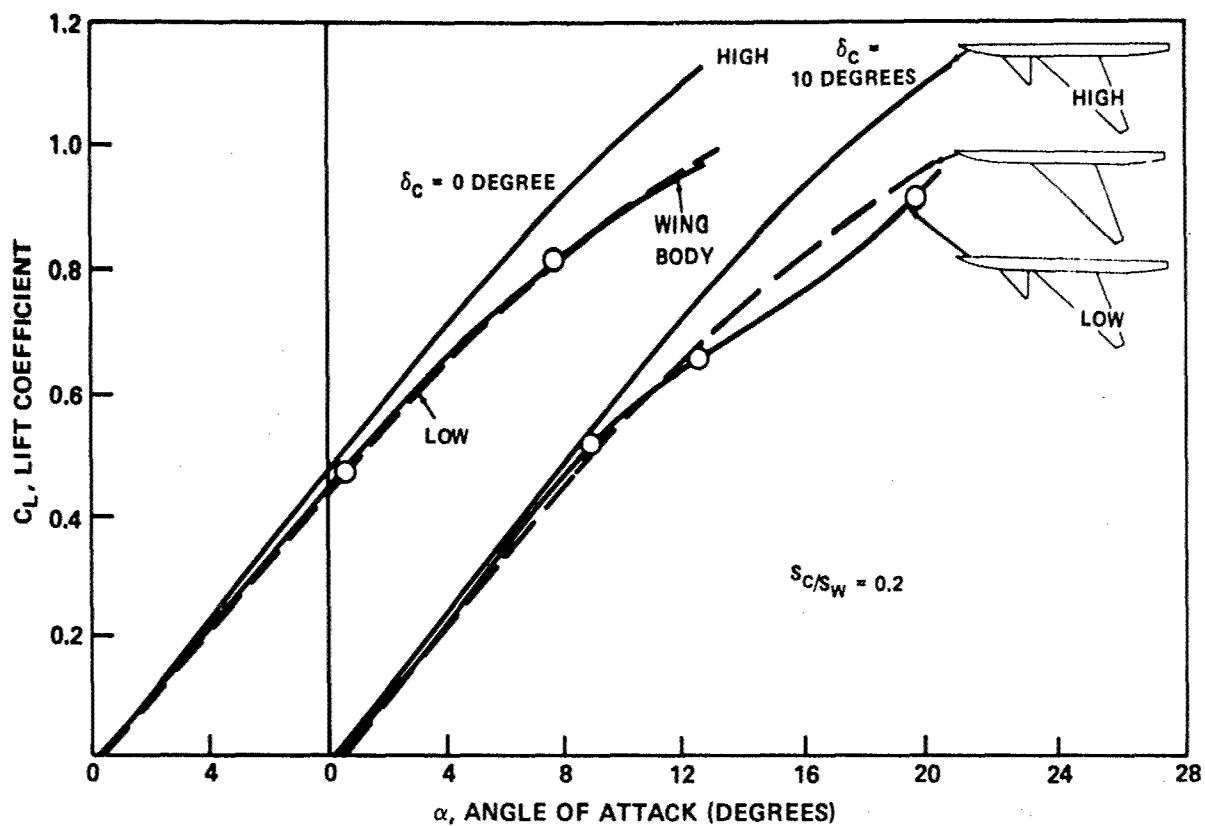
Figure 5a - Lift Coefficient
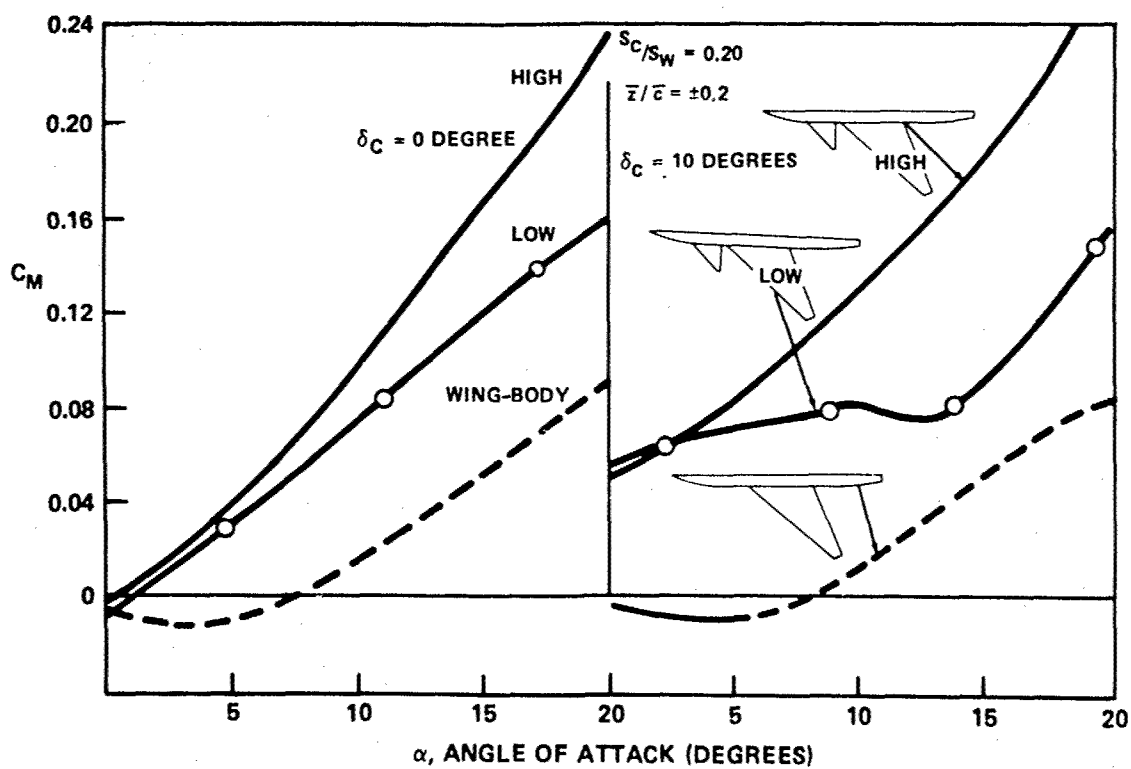
Figure 5b - Pitching Moment Coefficient

Figure 5 - Lift and Pitching Moment Coefficient Variation
due to Canard Vertical Location

Figure 6 - Sketch of 50-Degree Research Model

Figure 7 - Incremental Pitching Moment Coefficient Variation
due to Canard Vertical Location

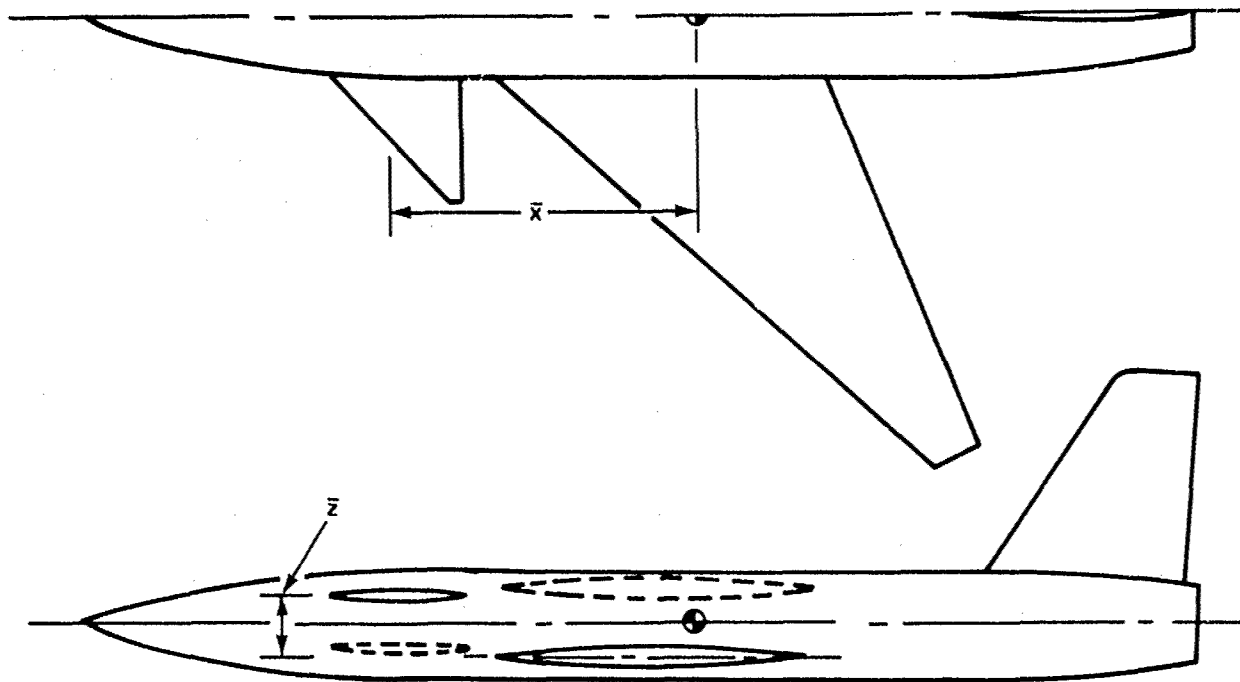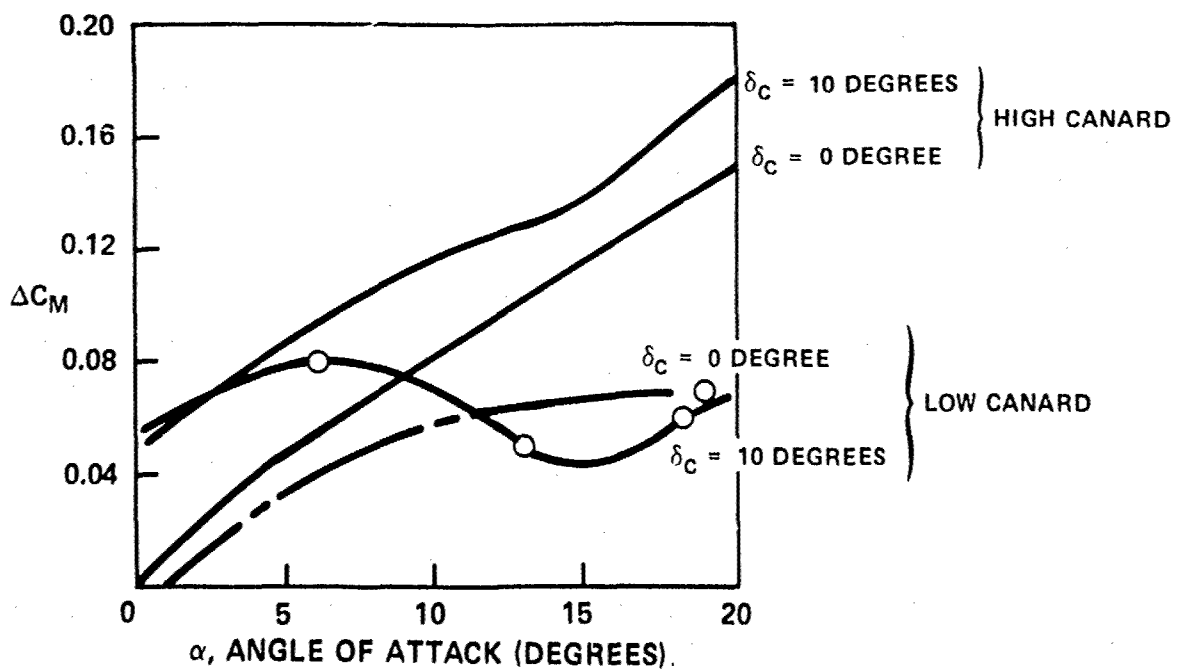Figure 8 - Lift, Drag, and Pitching Moment Coefficient
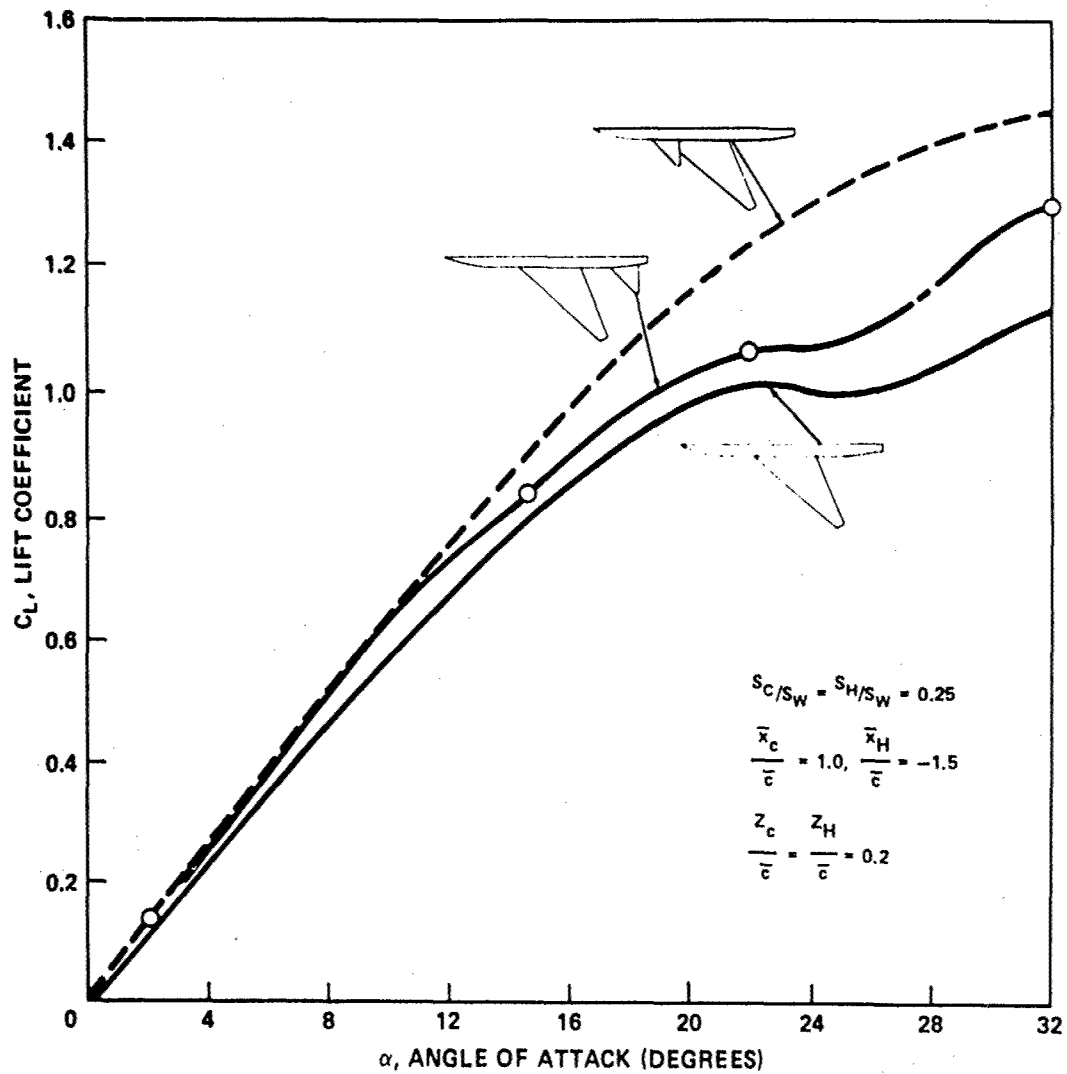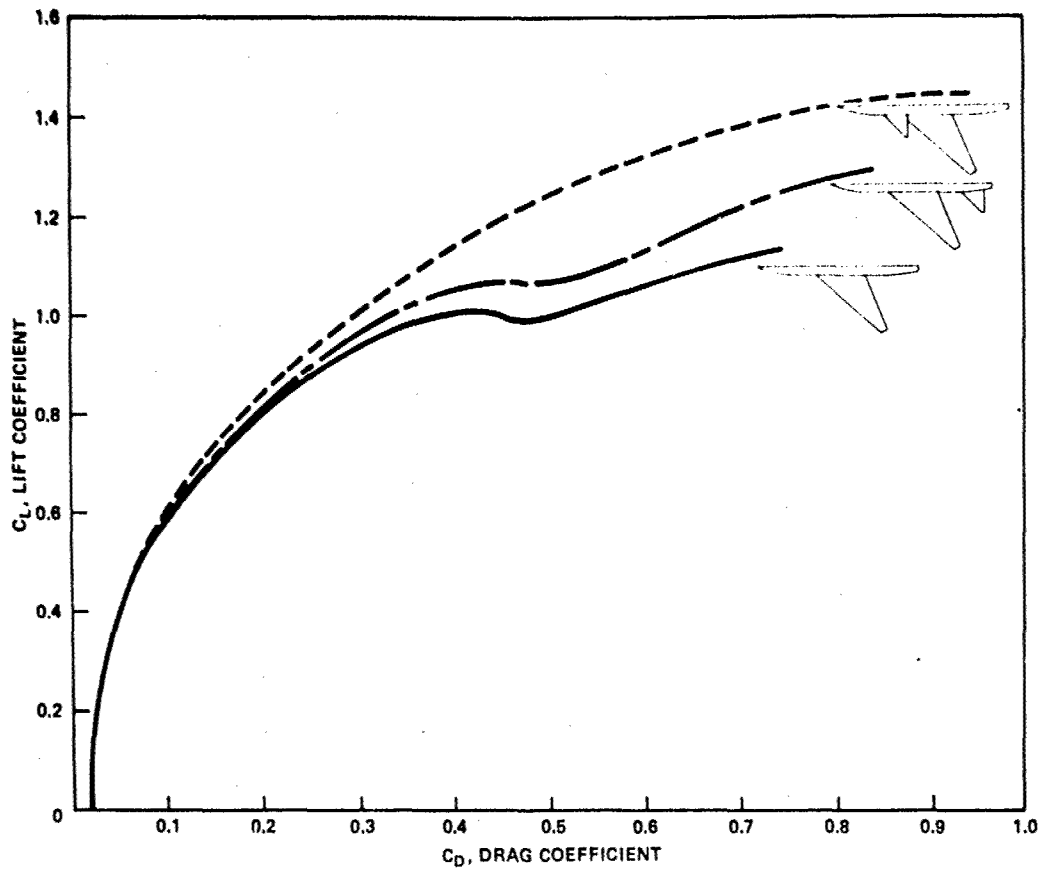due to Canard and Horizontal Tail

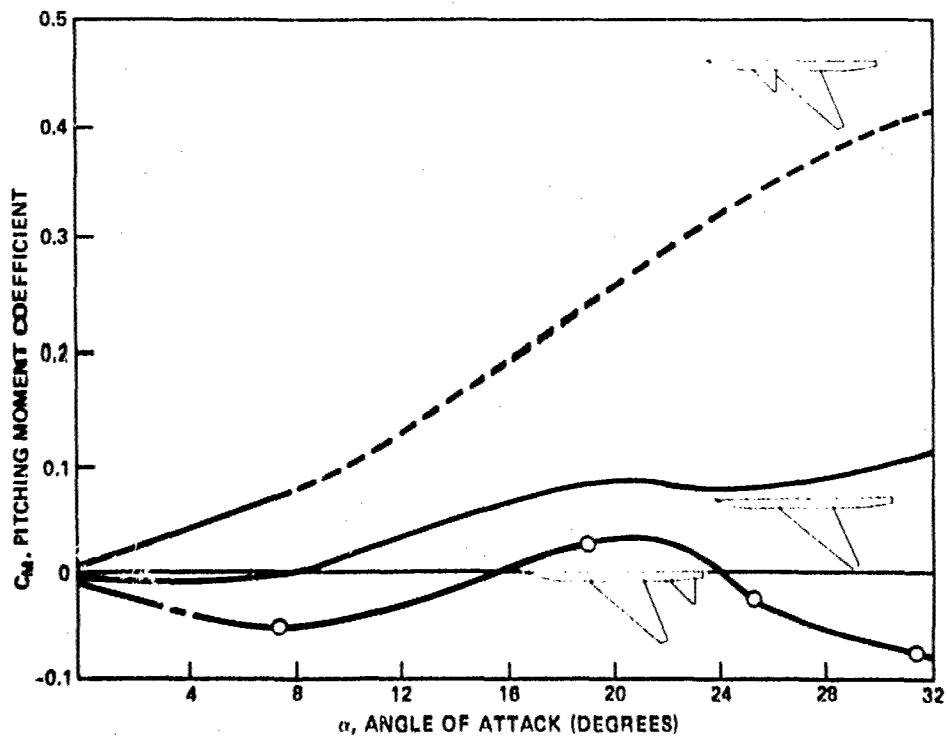Figure 8a - Lift Coefficient

Figure 8b - Drag Coefficient

Figure 8c - Pitching Moment Coefficient

12

planform as the canard and is located at an x/c of -1.5 aft of the 27 percent $\bar{c}$ and at $\bar{z}/\bar{c}$ = 0.2. The area ratio of both horizontal and canard surfaces $(S_H/S_w) = (S_c/S_w)$ is 0.25.

The plot of C_L versus α indicates both canard and tail have approximately the same lift curve slope at angles of attack less than 10 degrees. At greater angles, the canard has a larger slope and continues lifting up to 33 degrees.

Stall of the basic wing and wing-horizontal tail occur at approximately 21 degrees, whereas there is no hint of a stall for the canard up to 33 degrees.

The moment characteristics show the stall characteristics in a similar manner; there is a nose down pitching moment change of 21 degrees for both wing and wing-horizontal tail but no indication of change for the canard configuration.

Examination of the drag data indicates that the drag is less for the canard configured vehicle than for the wing-horizontal tail vehicle. This reduction in drag results in maneuvering gains. The canard configuration has lower drag at lift coefficients greater than 0.5 for the wing configuration and 0.65 for the wing-tail configuration, respectively.

The incremental lift and moment characteristics for canard and tail, presented in Figure 9, show the large increase in lift obtainable as well as the moment linearity associated with the canard. It is interesting to note that there is a region between α = 8 to 22 degrees where there is no change in incremental lift, thus indicating, for the horizontal tail, that the downwash from the wing is increasing at the same rate as the angle of attack.

INTERFERENCE

To determine the amounts of favorable or unfavorable interference between canard-wing and wing-tail, a series of buildup data was obtained. The buildup was done utilizing the 50-degree wing model and the 0.25-area ratio canard and horizontal tail. These data, presented in Figure 10, are representative of all canard and horizontal tail positions with the
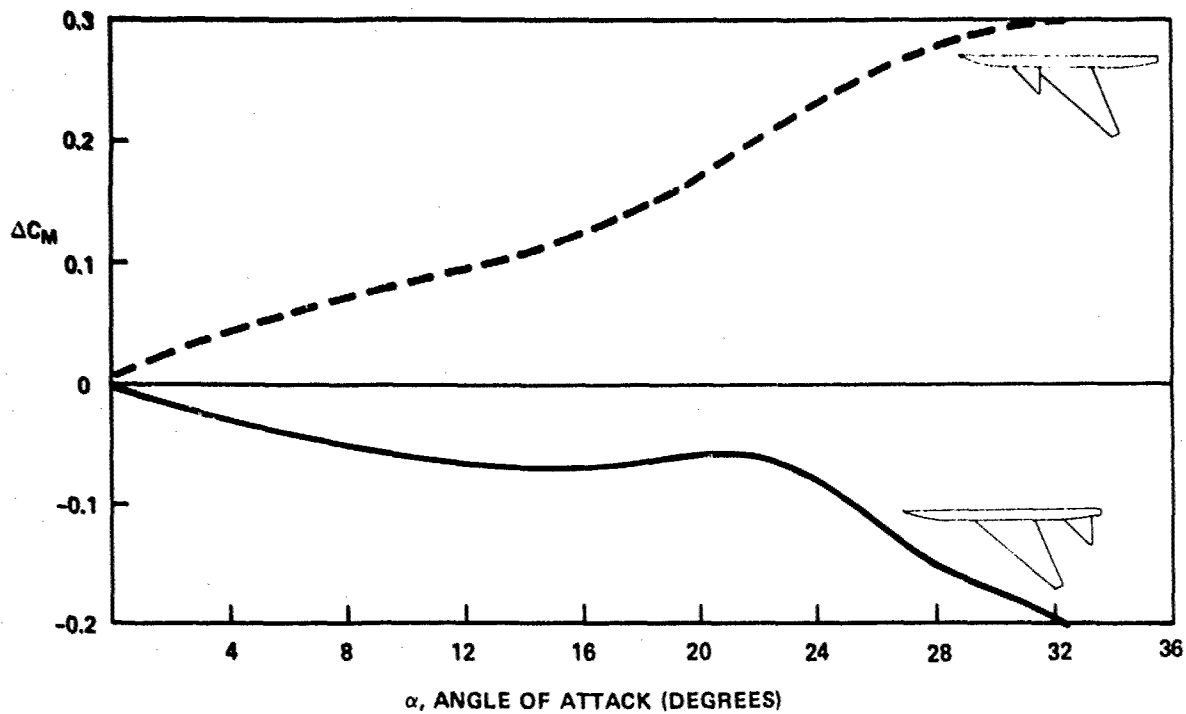
Figure 9a – Incremental Pitching Moment Coefficient
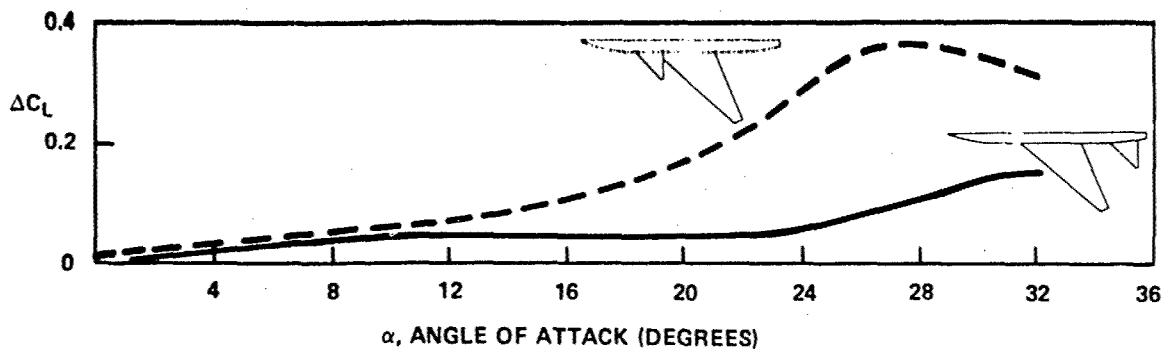
Figure 9b – Incremental Lift Coefficient

Figure 9 – Incremental Lift and Moment Coeffi<ient of
Canard and Horizontal Tail

exclusion of the increase in pitching moment with canard forward movement.
As indicated for either surface, there is little difference in incremental
lift between horizontal tail or canard and no stall.

These increments between body, body-canard, and body-horizontal tail
have been added to the basic wing-body and are shown in Figure 11 as are
the measured data for the complete configuration. The plots show the areas

14

Figure 10a – Lift Coefficient

Figure 10b – Pitching Moment Coefficient

Figure 10c – Drag Coefficient

Figure 10 – Lift, Drag, and Moment Characteristics of Body,
Body-Canard, and Body-Horizontal Tail

15

Figure 11 - Interference Effects of Canard and Horizontal Tail

Figure 11a - Lift Coefficient

Figure 11b - Drag Coefficient

Figure 11c - Pitching Moment Coefficient

17

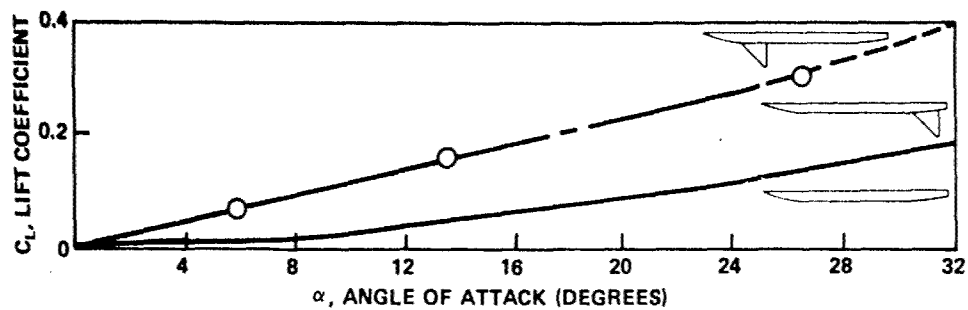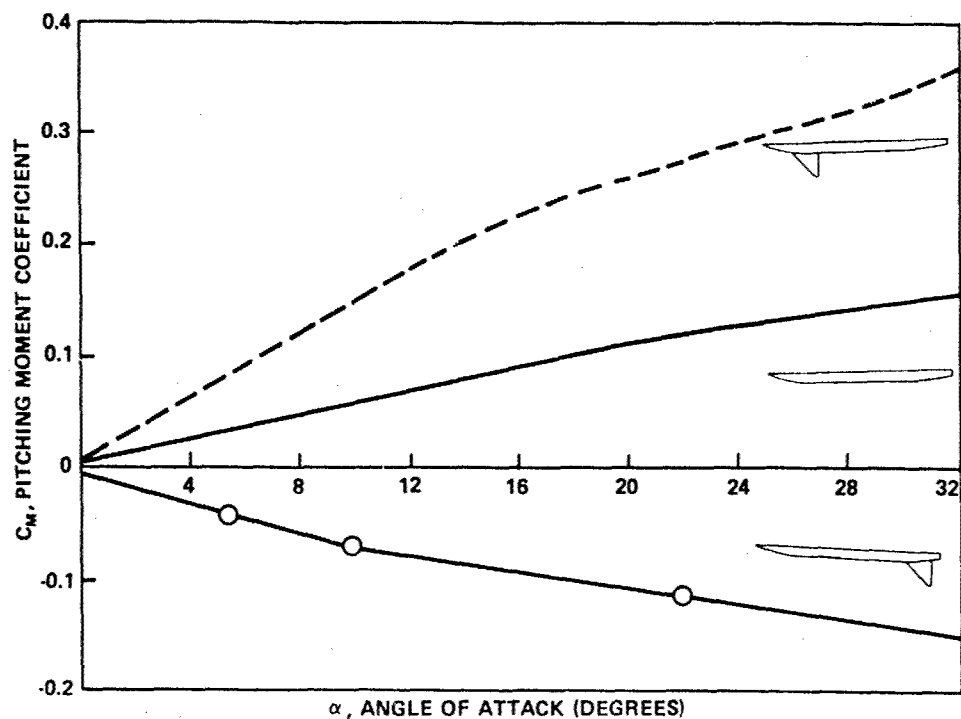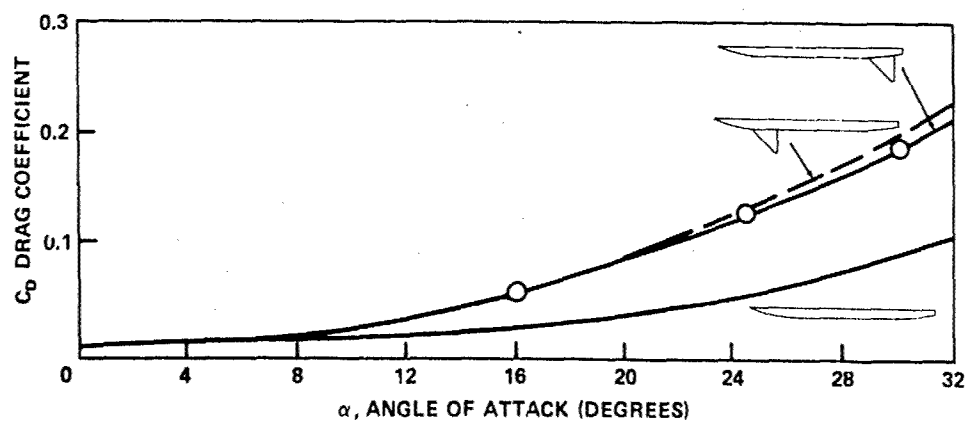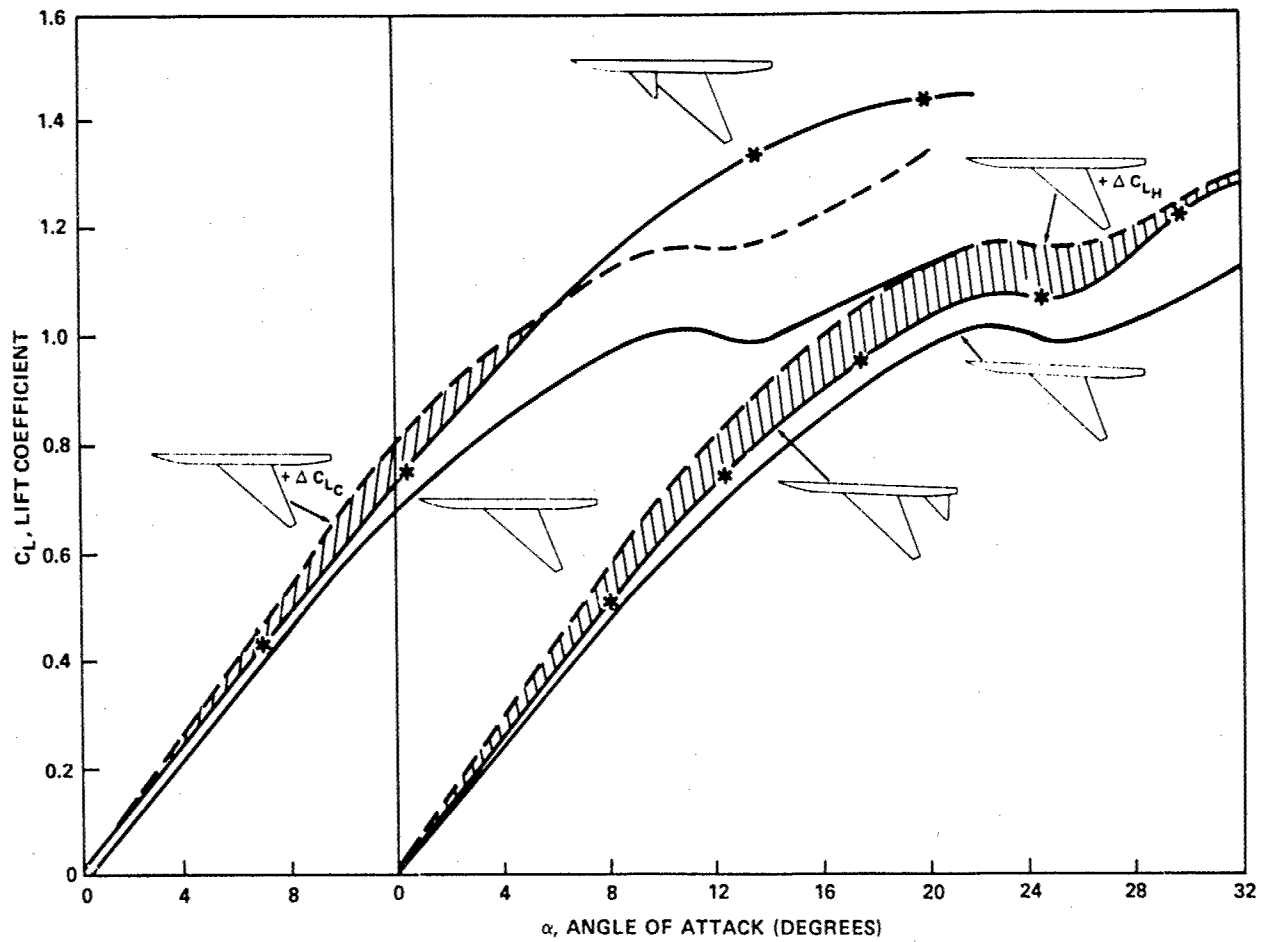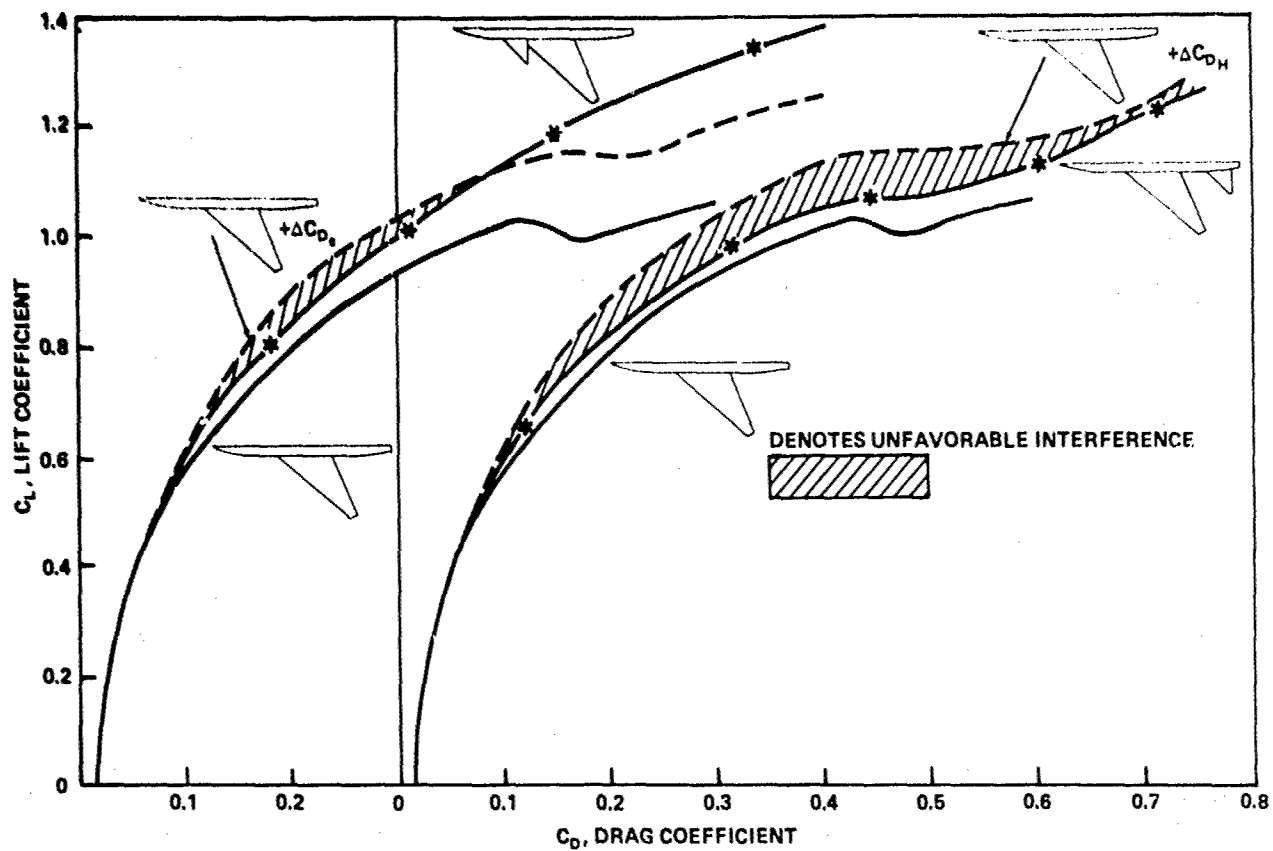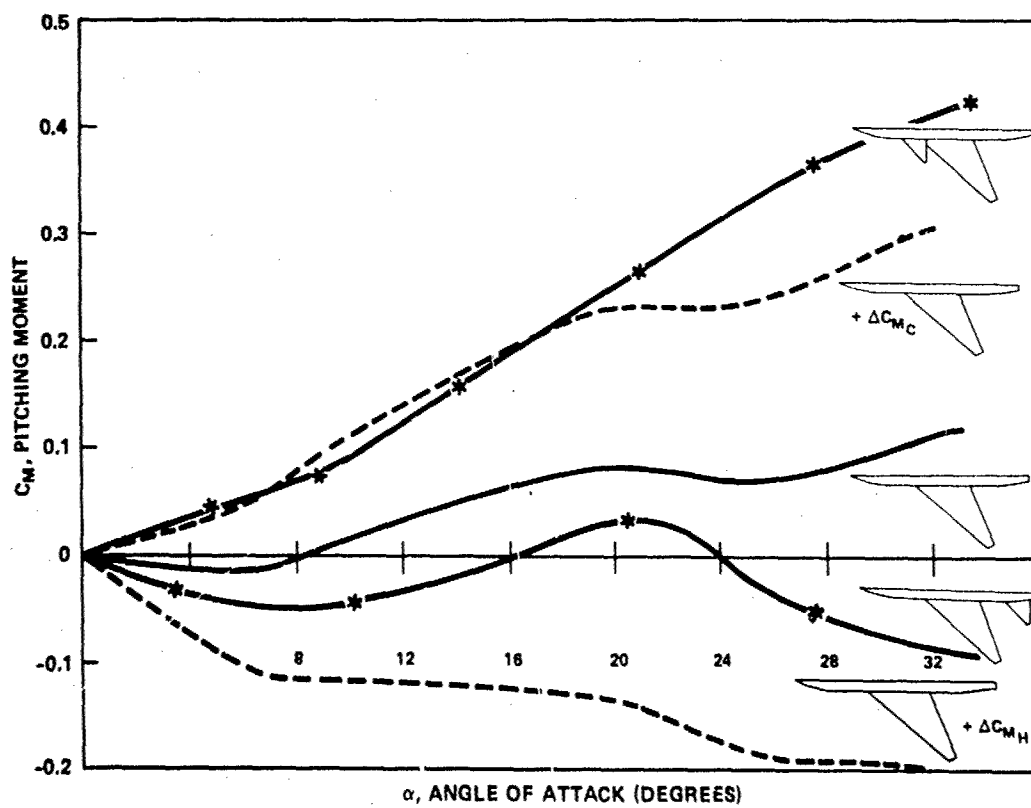of favorable or unfavorable interference. The canard configuration shows an unfavorable interference at angles of attack below 18 degrees. This interference is due to the downwash of the canard impinging on the wing thus causing a loss of wing lift. At angles of attack greater than 18 degrees, favorable interference occurs because the downwash from the canard delays wing stall and hence the overall configuration lift is increased. The tail shows an expected unfavorable interference throughout the angle of attack range because it is located in the downwash of the wing.

The drag data show similar trends for C_L between 0.5 and 1.1 ($8 < \alpha < 18$). There is an unfavorable interference for the canard in that the overall drag is higher than the sum of the components; however, at C_L greater than 1.1 there is favorable interference. The tail configuration once again had unfavorable interference at C_L greater than 0.5.

The moment characteristics show the effects of upwash or downwash on both canard and horizontal tail. The comparison between measured data and incremental data for the canard show little change between the two, thus indicating very little upwash on the canard at angles of attack up to 18 degrees. Comparison between measured and incremental tail configuration shows a greater variance due to the extensive downwash behind the wing.

WING SWEEP

As stated in the introduction, Navy aircraft, in general, have moderate-to-low swept wings. In order to investigate the effect of wing sweep on canard-wing characteristics, a comparison was made between the 50-degree swept wing and a 25-degree swept wing of similar planform.

A comparison between the two model geometries is shown in Figure 12; the body is the same for both models. The 25-degree wing has a 65A008 airfoil. The canard geometry is the same for both models and is located at $\bar{x}/\bar{c} = 1.0$. A detailed description of both models is given in the Appendix.

Comparison data for both basic wing-body and wing-body-canard are presented in Figure 13. As expected, there is an increase in lift curve slope for the 25-degree wing model but with stall occurring at 12 degrees rather than at 20 degrees for the 50-degree wing. The canard increases
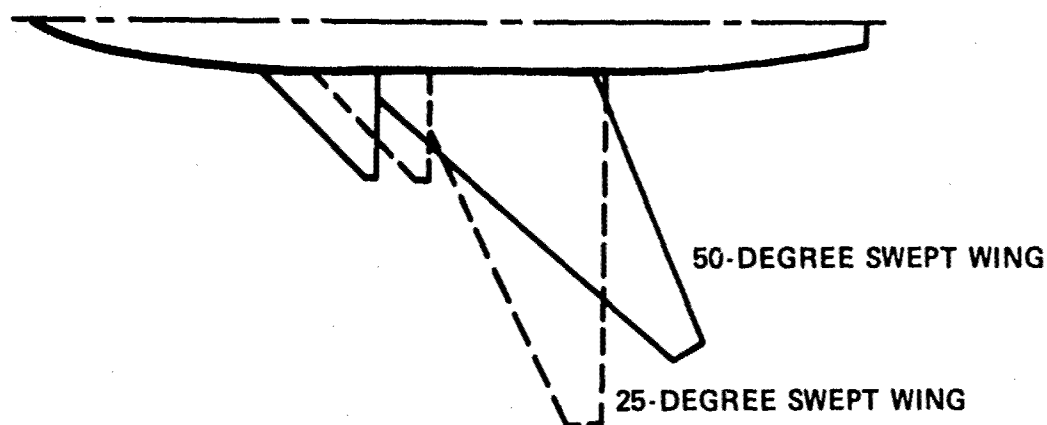
50-DEGREE SWEPT WING

25-DEGREE SWEPT WING

Figure 12 - Comparison between 25- and 50-Degree Swept
Wing Research Models

both the overall lift and angle of stall for both wings. Examination of the incremental lift shown in Figure 14 indicates that the amount of lift increase is nearly the same for both 25- and 50-degree wings.

The moment data in Figure 13 indicates little presence of stall when the canard is installed for either wing. The incremental data, shown in Figure 14, indicates linear pitching moment slopes for both configurations.

The drag data shows approximately the same drag reductions for both wings. The canard thus has favorable influences on the 25-degree wing as well as on the 50-degree wing.

The postulation in SAAB TN 60 is that there is a strong mutual vortex interaction between the canard and wing, both having highly swept delta configurations.

This explanation does not, however, indicate why a 45-degree canard can work on a 25-degree swept wing because neither wing nor canard can generate strong leading edge vortices. Thus, there must be an additional explanation for the canard-wing behavior. A possible explanation is that the downwash from the canard delays leading edge stall in a similar manner as a leading edge slot. Thus, the close-coupled canard might be thought of as a massive low-drag boundary layer device.

As evidence for this postulation, Figure 15 presents photographs of the 25-degree wing model with canard both on and off. As seen in the photo
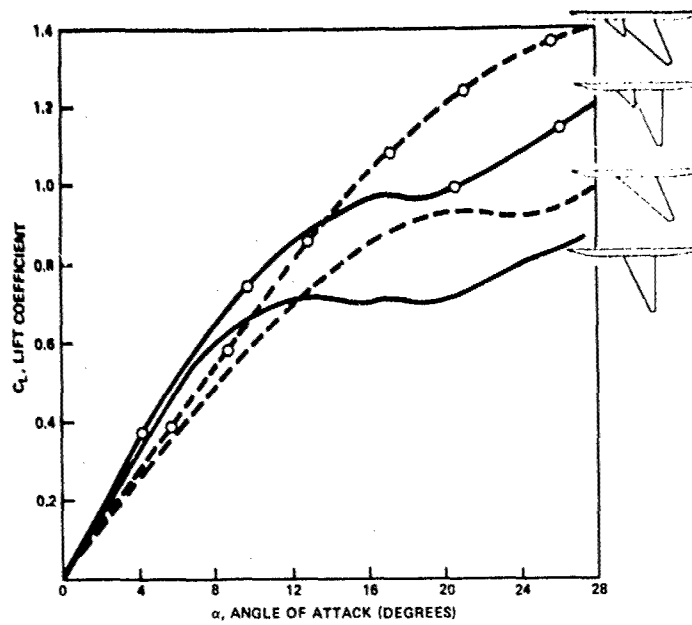
Figure 13a – Lift Coefficient
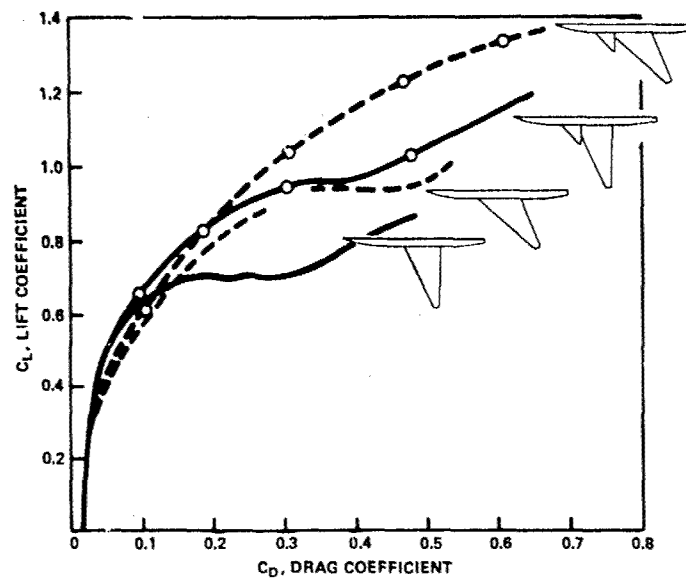
Figure 13b – Drag Coefficient
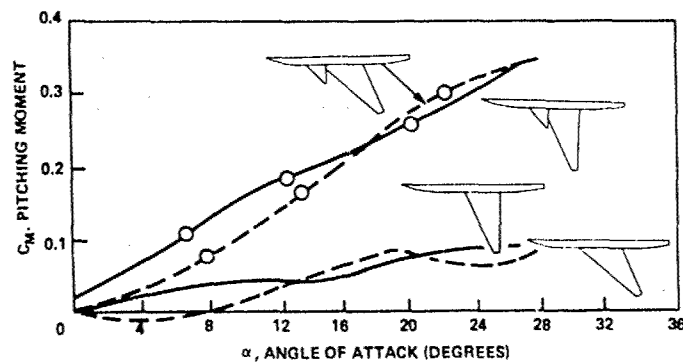
Figure 13c – Pitching Moment Coefficient

Figure 13 – Aerodynamic Characteristics of 25- and 50-Degree Research
Models Both with and without Canards
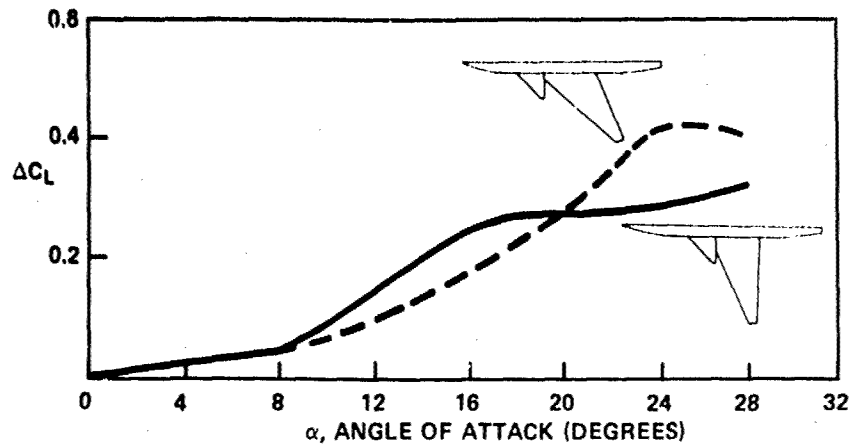
Figure 14a - Incremental Lift Coefficient
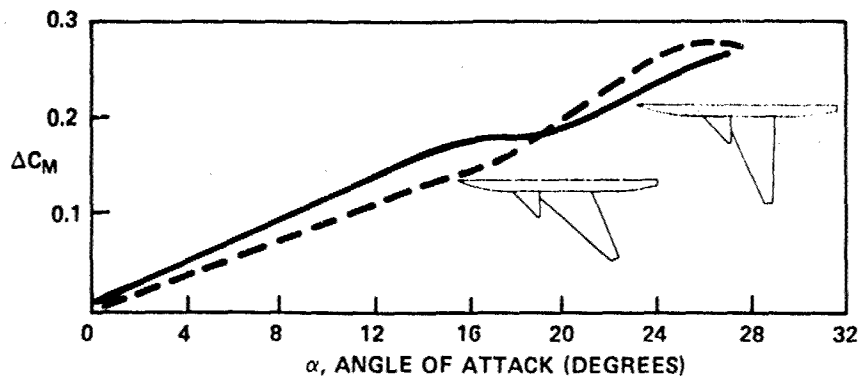
Figure 14b - Incremental Pitching Moment Coefficient

Figure 14 - Incremental Lift and Moment due to Canard on 25-
and 50-Degree Research Models

of the canard-off case, the tufts indicate wing stall which is correlated
with the actual force data. Adding the canard shows that the flow over
that portion of the wing aft of the canard is attached and, thus, not
stalled.

POSITION

The previous discussions have been based on the canard being in the
high position and generally at an $\bar{x}/\bar{c} = 1.0$. Longitudinal and vertical
position, however, have a strong effect on the various characteristics, and
will now be discussed for the 50-degree wing model.

21

Figure 15a - Canard Off

Figure 15b - Canard On (CO P3 DO)

Figure 15 - Effect of Canard on Flow of the 25-Degree Research Model

Seven different canard positions were evaluated on this model. These seven positions are shown in Figure 16. Position 1 (P_1) is the highest most forward location and P_7 is the lowest location. Positions 1, 2, and 3 are located at $\bar{z}/\bar{c} = 0.1$; P_7 is in the plane of the wing.

NOTE: ALL DIMENSIONS ARE IN INCHES (CENTIMETERS)
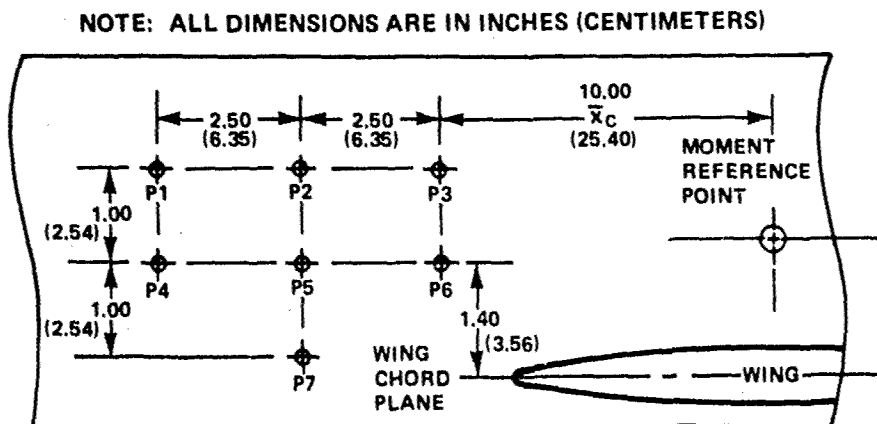
Figure 16 - Canard Position Ordinates

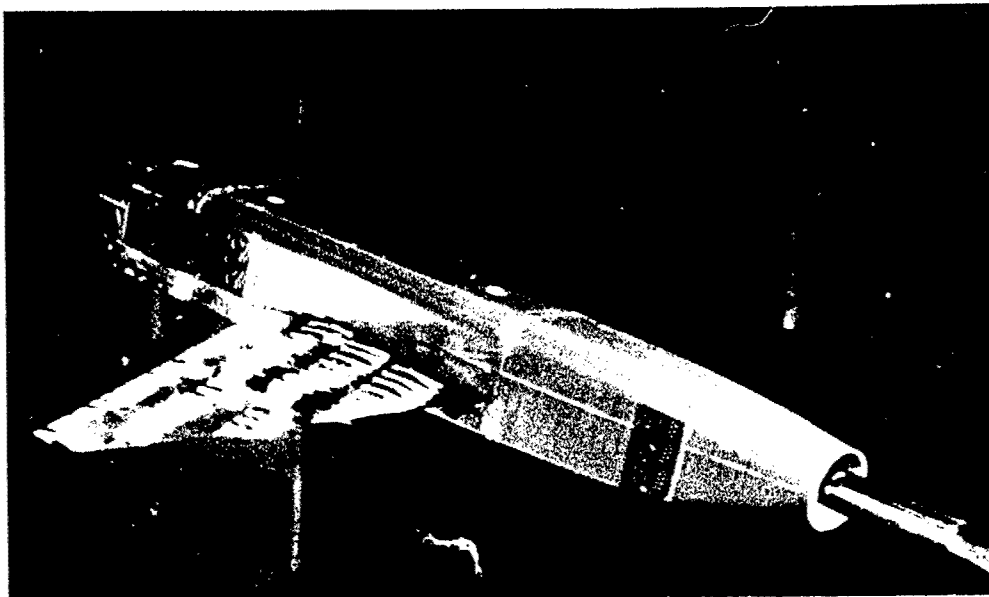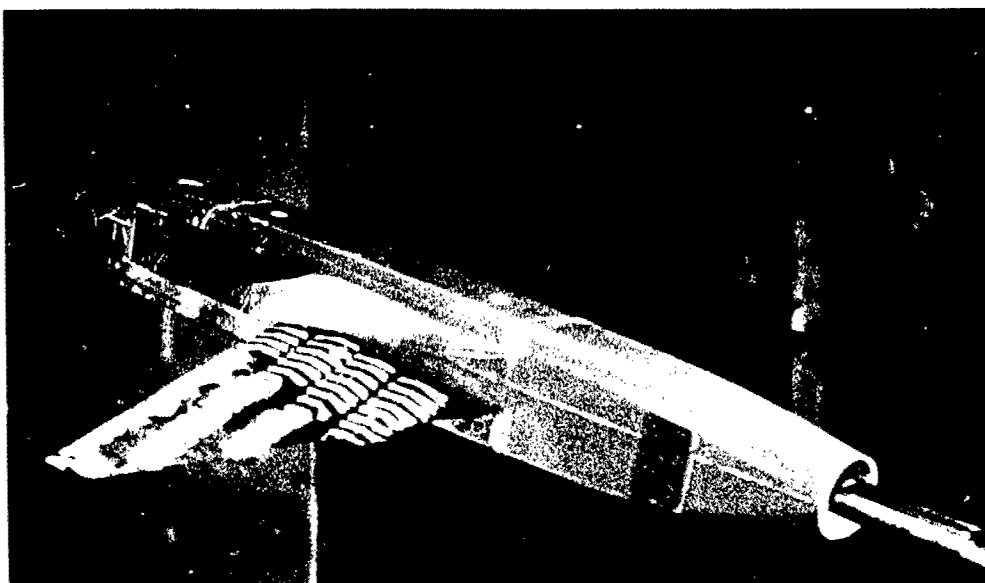Lift data are presented in Figure 17 for each of these positions. Maximum lift occurs at P_2 with a rapid dropoff and stall at P_1. Position 3 has a lower maximum lift than P_2, however no stall is evident.

Lowering the canard does not change these trends with longitudinal positions in that P_4 (most forward) has the lowest value of maximum lift. Maximum lift is further decreased when the canard is in the plane of the wing. This variation in $C_{L_{max}}$ is presented in Figure 18. The moment characteristics indicate the fairly linear characteristics throughout the angle of attack range. As expected, moving the canard forward causes a larger destabilizing moment. This destabilizing moment is somewhat reduced as the canard is brought closer to the plane of the wing. The moment data, shown in Figure 19, reflect the various lift characteristics of the different positions as there is a definite increase in pitching moment stability for the P_1 and P_4 configurations, thus indicating a loss in canard effectiveness.
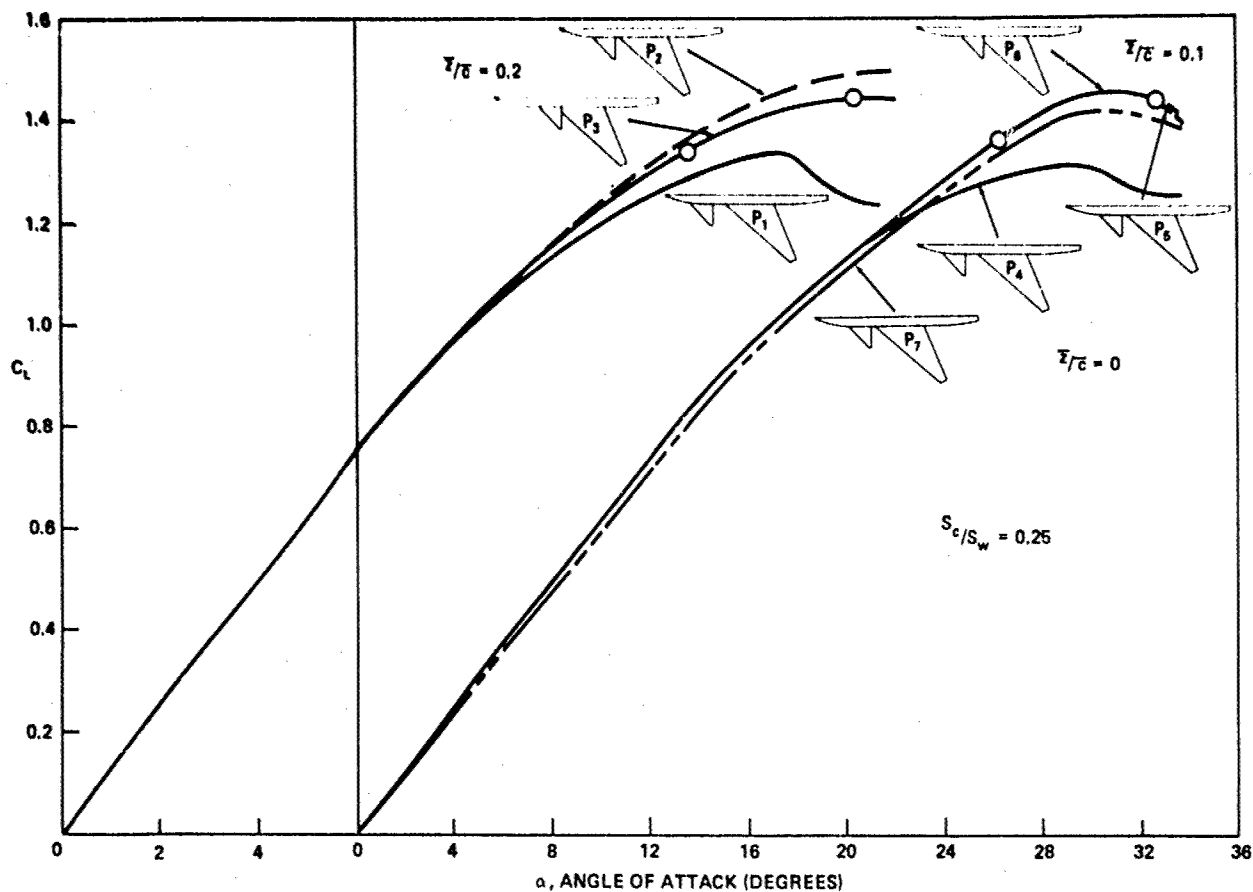
Figure 17 - Lift Coefficient Variation due to Canard Position
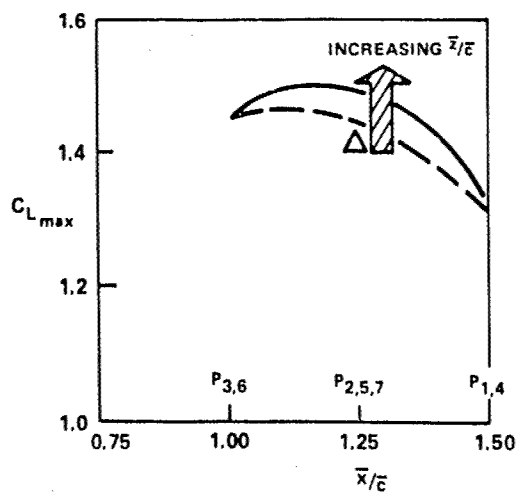
Figure 18 - Maximum Lift Coefficient Variation with Canard Position

24
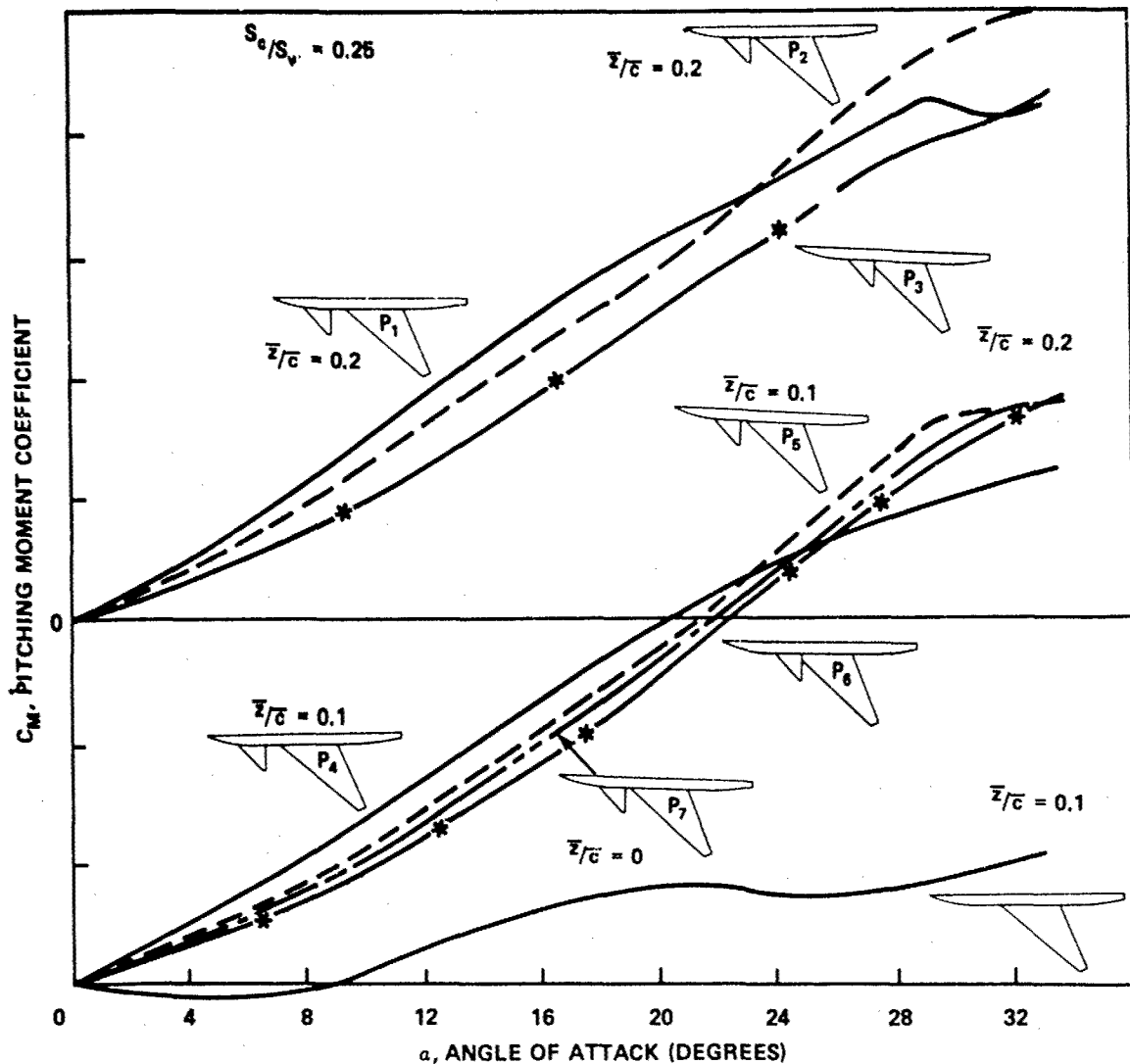
Figure 19 - Pitching Moment Coefficient Variation with Canard Position

Incremental moments are plotted in Figure 20, and indicate that at low angles the increase in C_M is generally proportional to the canard volume coefficient and that, aside from Positions 1 and 4, no canard stall is evident.

The effect of position on the drag characteristics is shown in Figure 21. At low lift coefficients there is little effect on C_D. Drag is increased at the higher values of C_L by moving the canard forward to Positions 1 and 4 or by lowering it. Up to the stall C_L of P_1 and P_4 the highest drag occurred for the canard in the plane of the wing P_7.
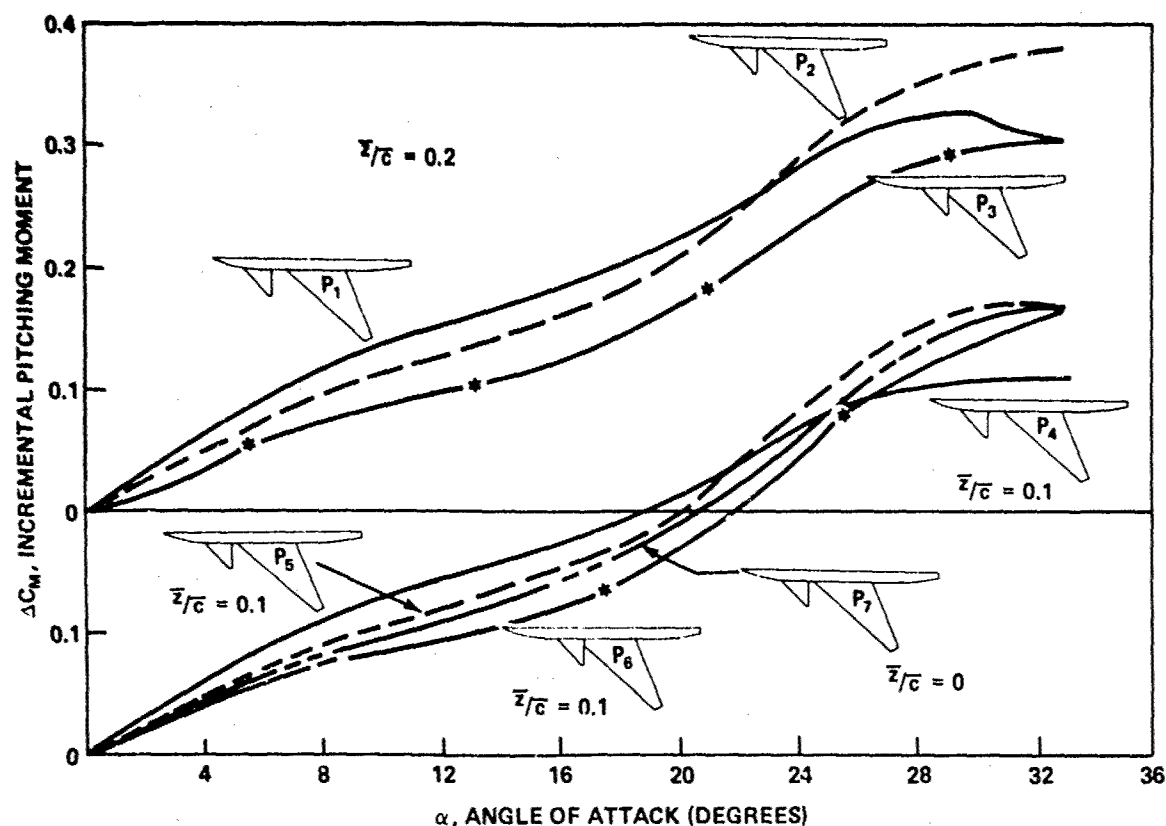
Figure 20 - Incremental Pitching Moment Coefficient Variation
with Canard Position

The variation of $(L/D)_{max}$ with position is shown in Figure 22. The
figure indicates that the greatest value of $(L/D)_{max}$ occurs at Positions 2
and 3 and the lowest value occurs at P_6. Also indicated is the fact that
lowering the canard reduces $(L/D)_{max}$. Similar trends are shown for minimum
drag C_{D_0} which is presented in Figure 23. Lowering the canard increased
minimum drag.

DEFLECTION

The effects of canard deflection on lift and maximum lift coefficient
are presented in Figures 24 and 25, respectively, for the 50-degree wing.
The canard has an area ratio of 0.25 and is located at P_3 ($\bar{z}/\bar{c} = 0.2$,

26
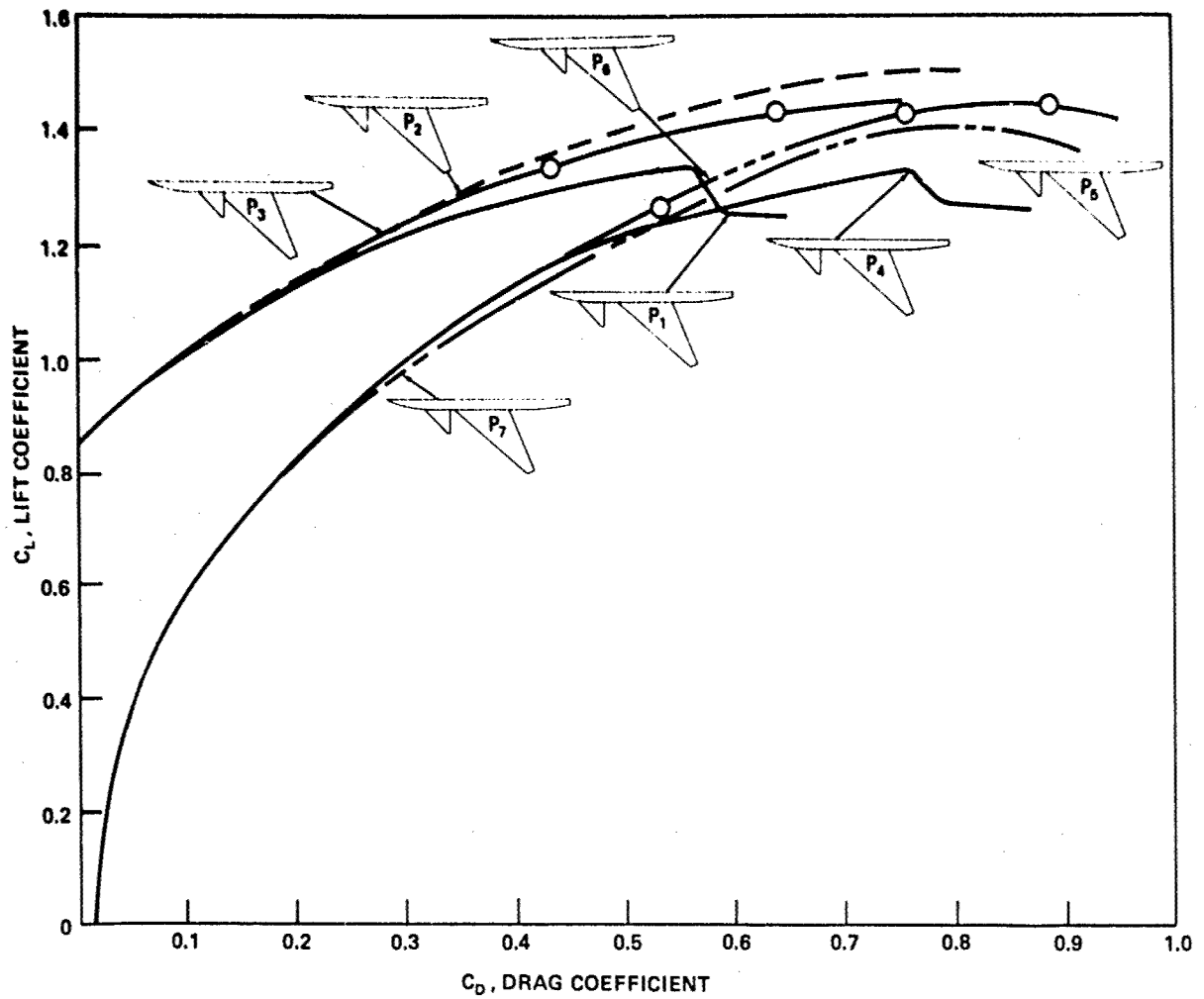
Figure 21 – Drag Coefficient Variation with Canard Position
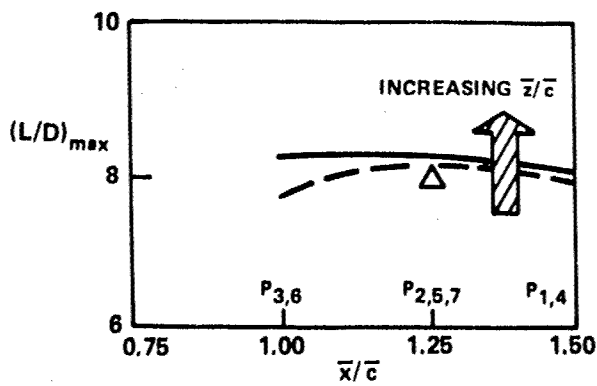
Figure 22 – Maximum Lift-to-Drag
Ratio with Canard Position
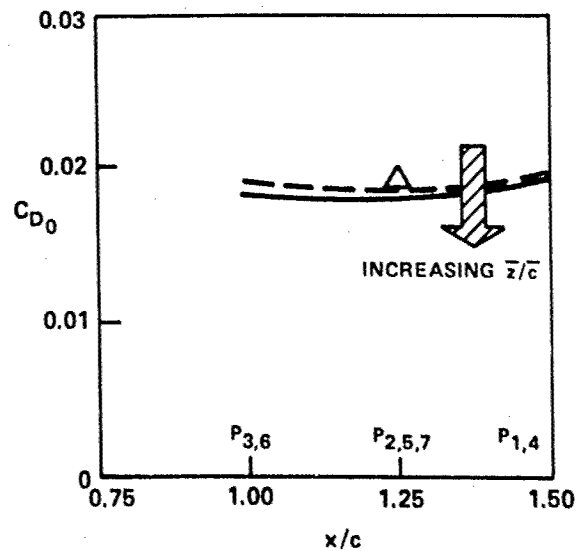
Figure 23 – Minimum Drag Coefficient
Variation with Canard Position

$\bar{x}/\bar{c} = 1.0$). Deflection of the canard does not appreciably increase or decrease lift for the range of deflections that would be expected. In fact, $C_{L_{max}}$ changed only 0.08 between -10 to +10 degrees deflection. The variation in C_L at 5 degrees is shown in Figure 26. This indicates, again, that half the lift generated by the canard deflection is lost due to interference of the additional downwash on the wing.
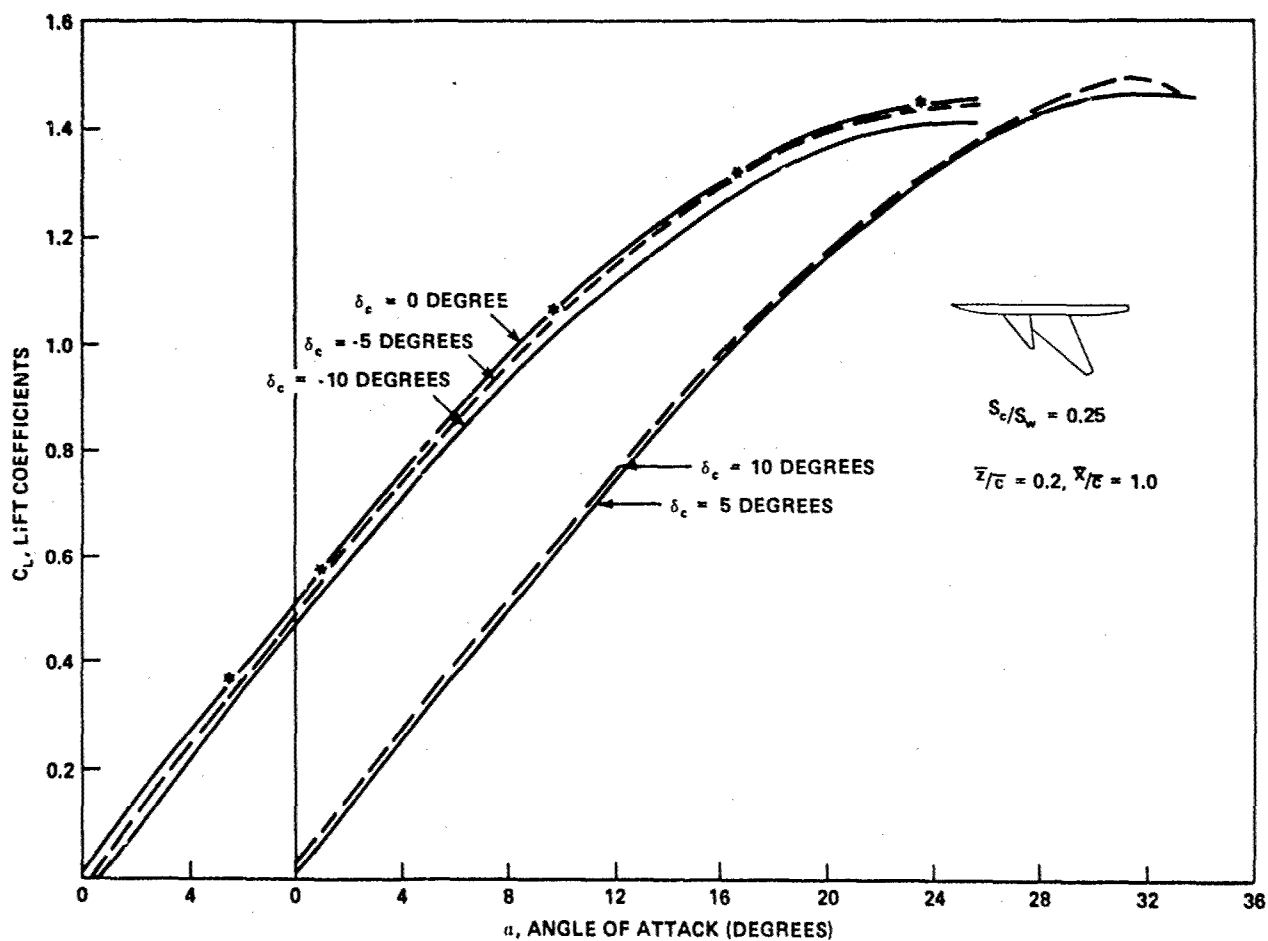
Figure 24 - Effect of Canard Deflection on Lift Coefficient
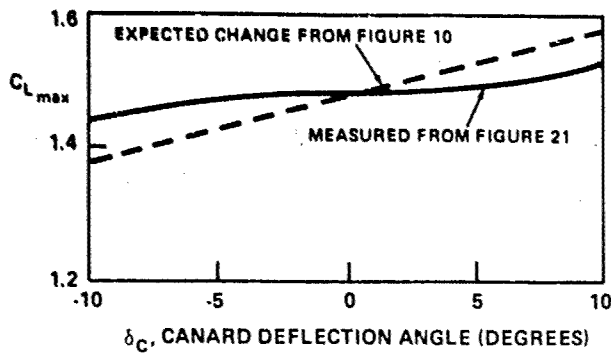
Figure 25 - Effect of Canard Deflection on Maximum Lift Coefficient
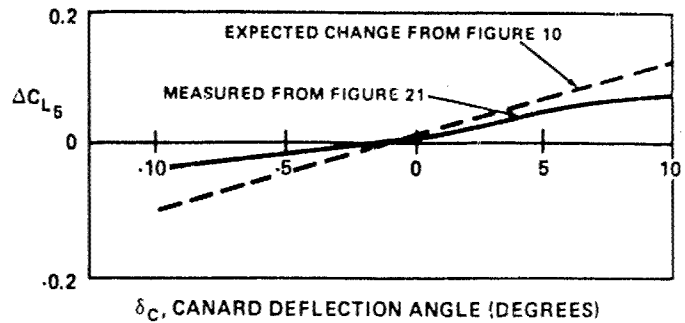
Figure 26 - Effect of Canard Deflection on Incremental Lift Coefficient at 5-Degrees Angle of Attack

The effect on drag due to deflection is shown in Figure 27. The variations of C_{D_0} and $(L/D)_{max}$ are shown in Figures 28 and 29, respectively. As shown, positive deflections increase drag at practically all lift coefficients. This increase in drag leads to a marked reduction in $(L/D)_{max}$. Small negative deflections actually improved $(L/D)_{max}$, while not increasing C_{D_0}.

The slight increase in $(L/D)_{max}$ is due to the fact that $(L/D)_{max}$ occurs at approximately 5-degrees angle of attack. Thus, when the canard is at approximately 0-degree local angle of attack, induced canard drag is minimized.

Pitching moment and the variation of ΔC_M with δ_c are shown in Figures 30 and 31. The moment data indicates that C_{M_δ} is relatively constant over the angle of attack range. The plot of ΔC_M indicates that the moment contribution due to canard deflection is approximately half that due to canard angle of attack, i.e., $C_{M_\delta} = 1/2\ C_{M_\alpha}$.

SIZE

Much of the discussion up to this point has been limited to a canard-wing area ratio of 0.25. This was the maximum area ratio tested on the 50-degree research model. Three other geometrically similar 45-degree
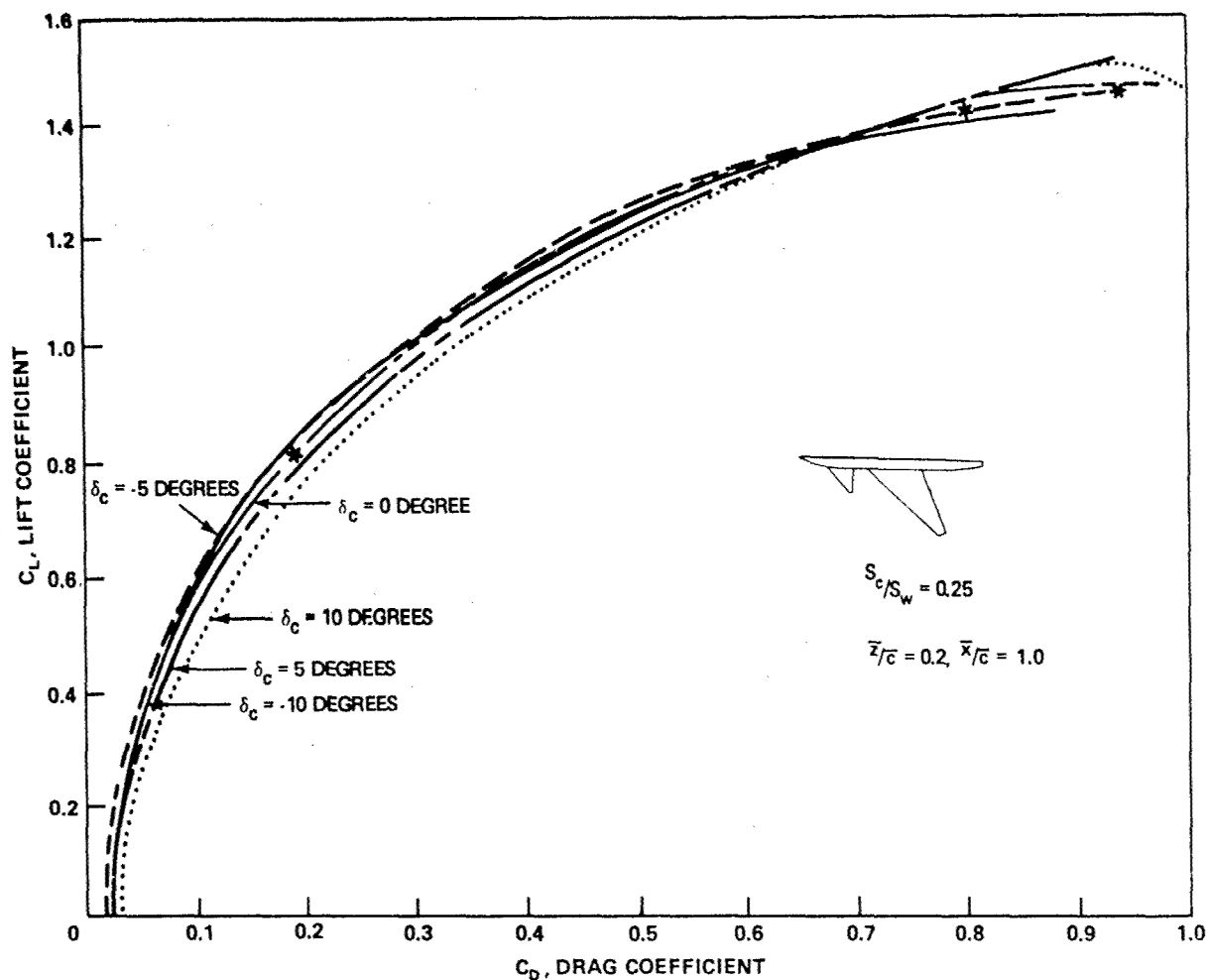
Figure 27 - Effect of Canard Deflection on Drag Coefficient

truncated delta canards were also evaluated and are shown in Figure 32.
Area ratios for the three were 0.1, 0.15, and 0.20. Data for all four
configurations are presented in Figures 30, 31, and 32. Figure 33 presents
the variation of C_L with size. The increase in C_L is fairly linear with
increasing canard size. Figure 34 presents the variation in C_L evaluated
at 20-degrees angle of attack for the three upper positions. At each
position the increase in C_L is also relatively linear.
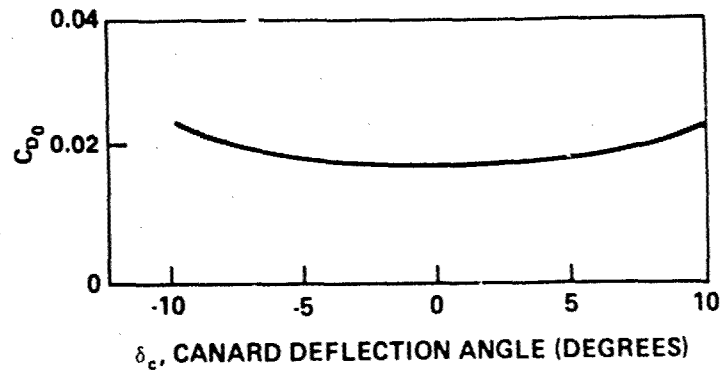
Figure 28 – Effect of Canard Deflection on Minimum Drag Coefficient
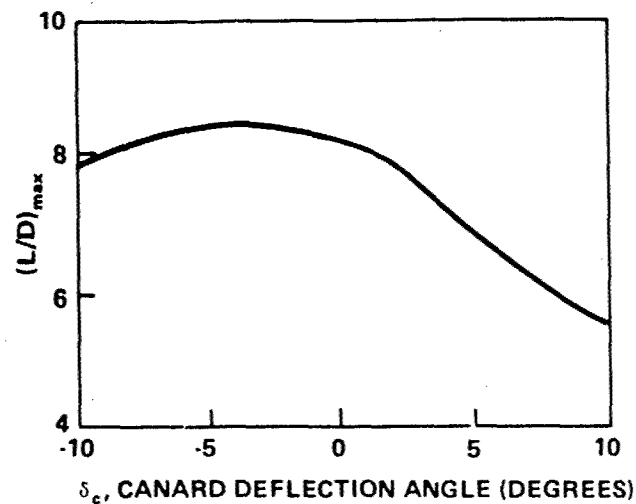
Figure 29 – Effect of Canard Deflection on Maximum
Lift-to-Drag Ratio

Figure 35 presents incremental moment data for P_1 and P_2 at C_L values of 0.4 and 0.8. Once again the increase in moment is reasonably linear with canard size. As stated earlier, an area ratio of 0.25 was the largest canard evaluated, and judging from the linearity of the results, it would be tempting to increase the area ratio further. Data from SAAB TN 60 indicates that at area ratios much greater than 25 percent there is a sharp dropoff in the effective increase in lift with canard size.

PLANFORM

All of the previous discussion has been based on the 45-degree truncated delta canard. Three other canards were evaluated and are shown in

31
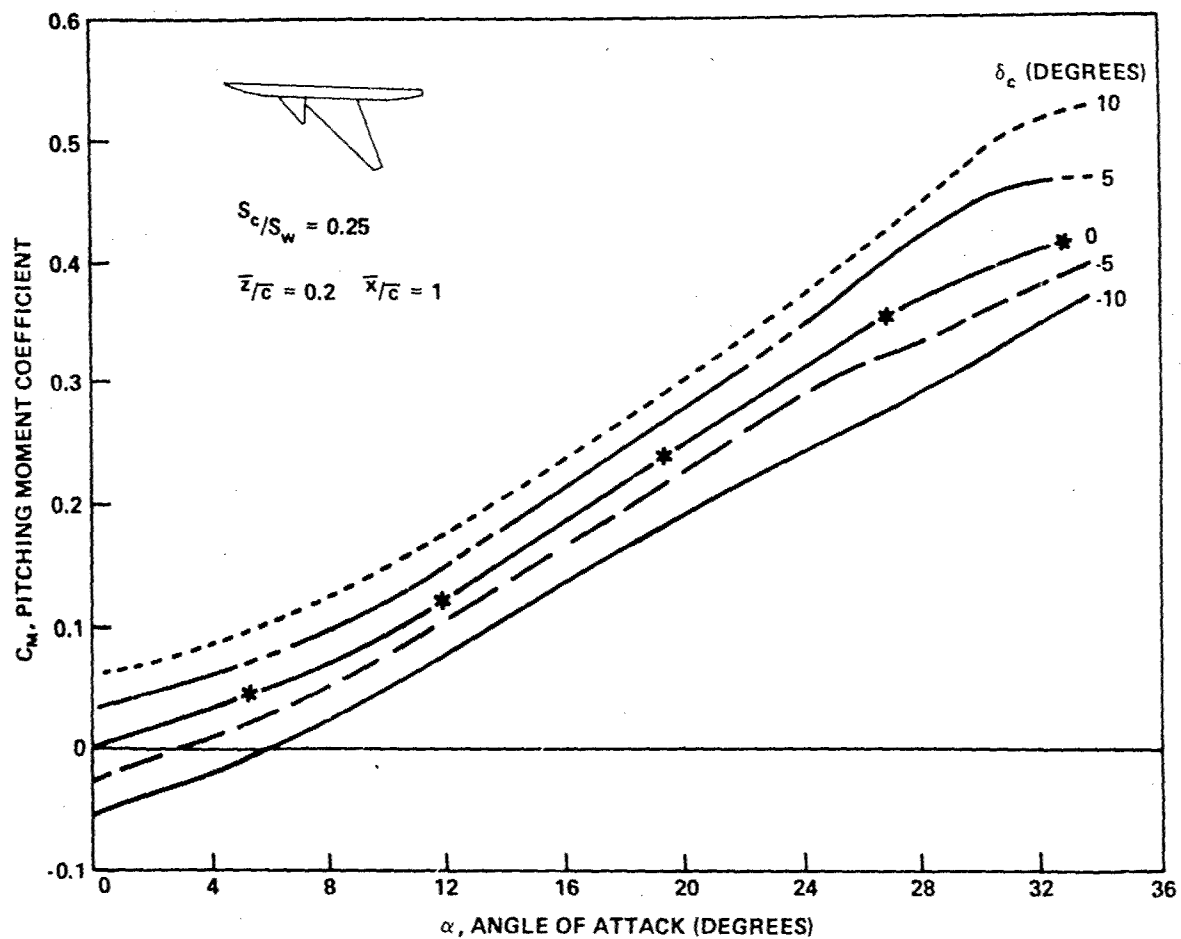
Figure 30 – Effect of Canard Deflection on Pitching Moment Coefficient
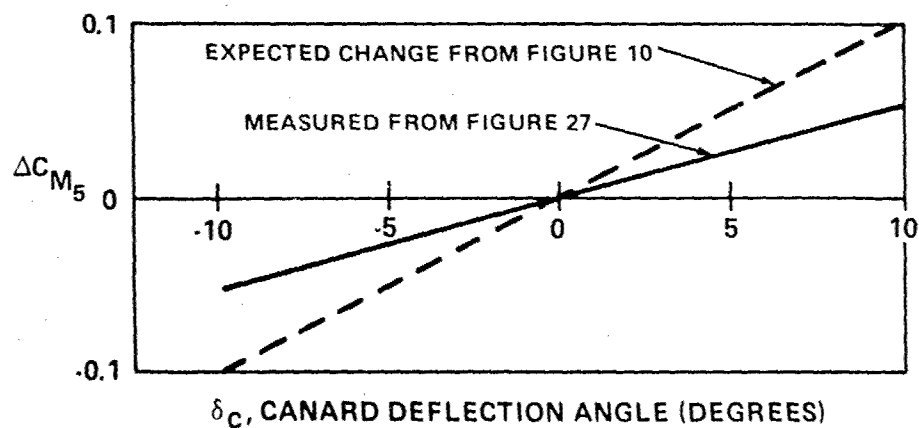
Figure 31 – Effect of Canard Deflection on Incremental Pitching
Moment Coefficient of 5-Degrees Angle of Attack

32
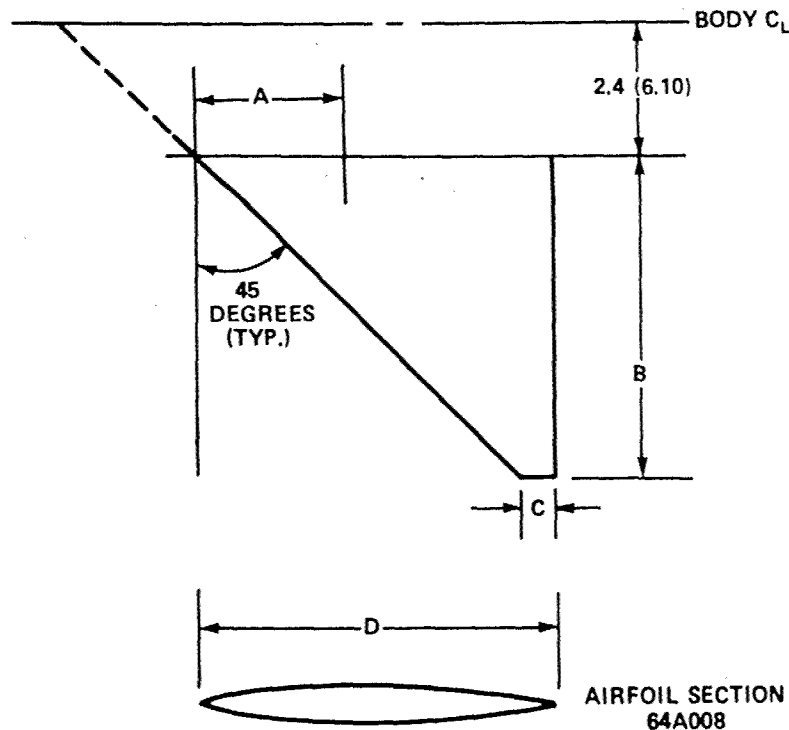
S_c/S_w	PIVOT DISTANCE A		SPAN B		TIP CHORD C		ROOT CHORD D		CANARD AREAS	
	IN.	CM.	IN.	CM.	IN.	CM.	IN.	CM.	IN.^{2}	CM.^{2}
0.10	1.38	3.51	2.74	6.96	0.38	0.97	3.12	7.92	30.5	196.8
0.15	1.75	4.44	3.91	9.93	0.44	1.12	4.35	11.05	45.7	294.8
0.20	2.25	5.72	4.84	12.29	0.56	1.42	5.40	13.72	61.0	393.5
0.25	2.62	6.65	5.74	14.58	0.59	1.50	6.33	16.08	75.8	489.0

Figure 32 - Geometrically Similar Canards

Figure 36. The three canards were 60-degree delta planform (C_1), a 45-degree high aspect ratio tapered planform (C_2), and a 25-degree high aspect ratio tapered planform (C_3). Pertinent dimensions of the canards are given in the Appendix.

Figure 37 presents the variation of $C_{L_{max}}$ with canard position for the four canards at all seven positions tested. The maximum lift

33
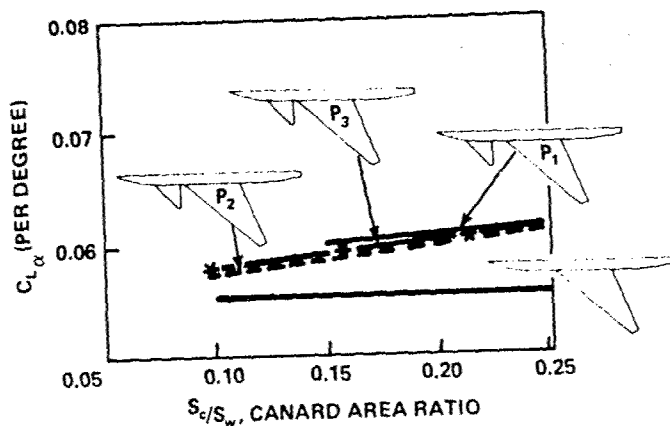
Figure 33 – Effect of Canard Size
on Lift Curve Slope
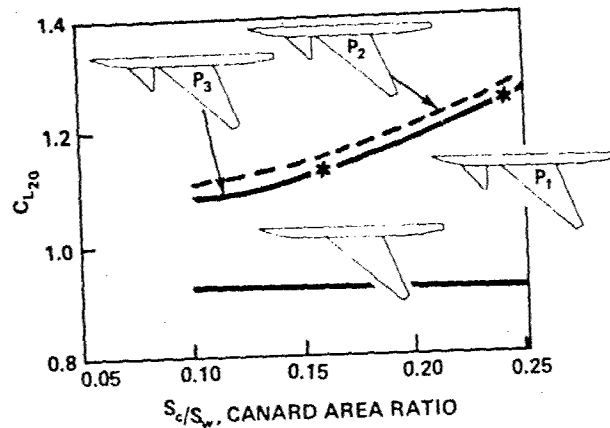
Figure 34 – Effect of Canard Size
on Lift Coefficient at 20-Degrees
Angle of Attack
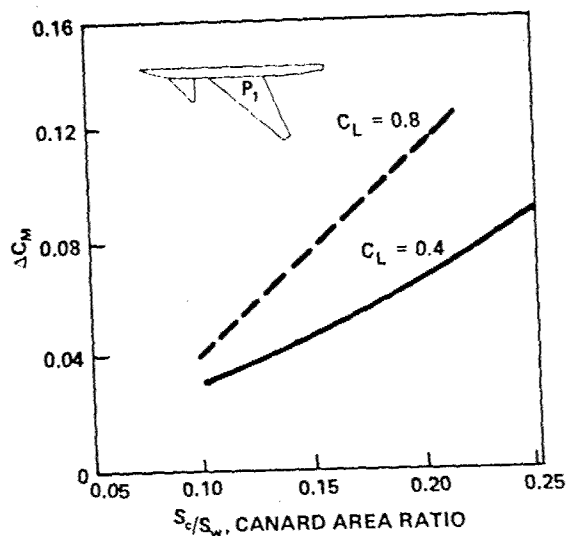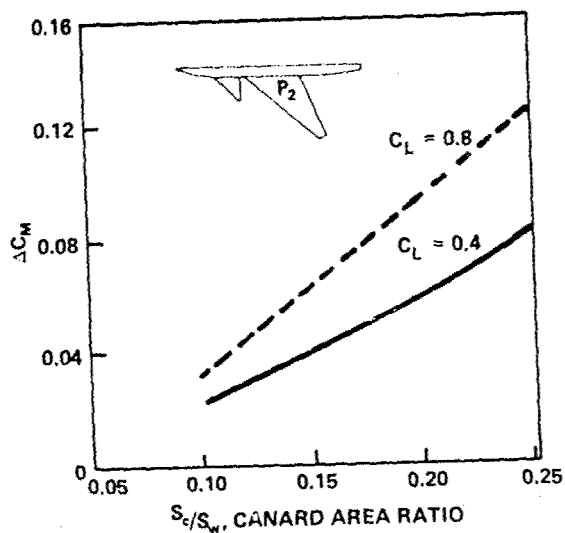
Figure 35 – Effect of Canard Size on Incremental Pitching
Moment Coefficient
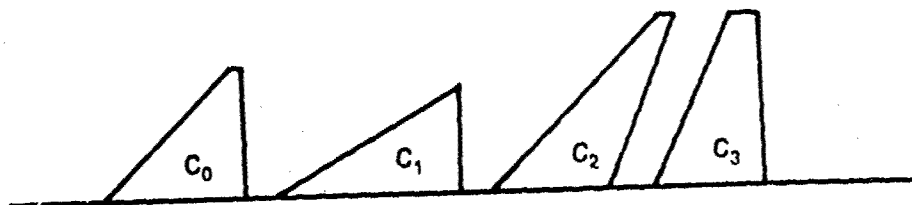
Figure 36 – Canard Planforms

34
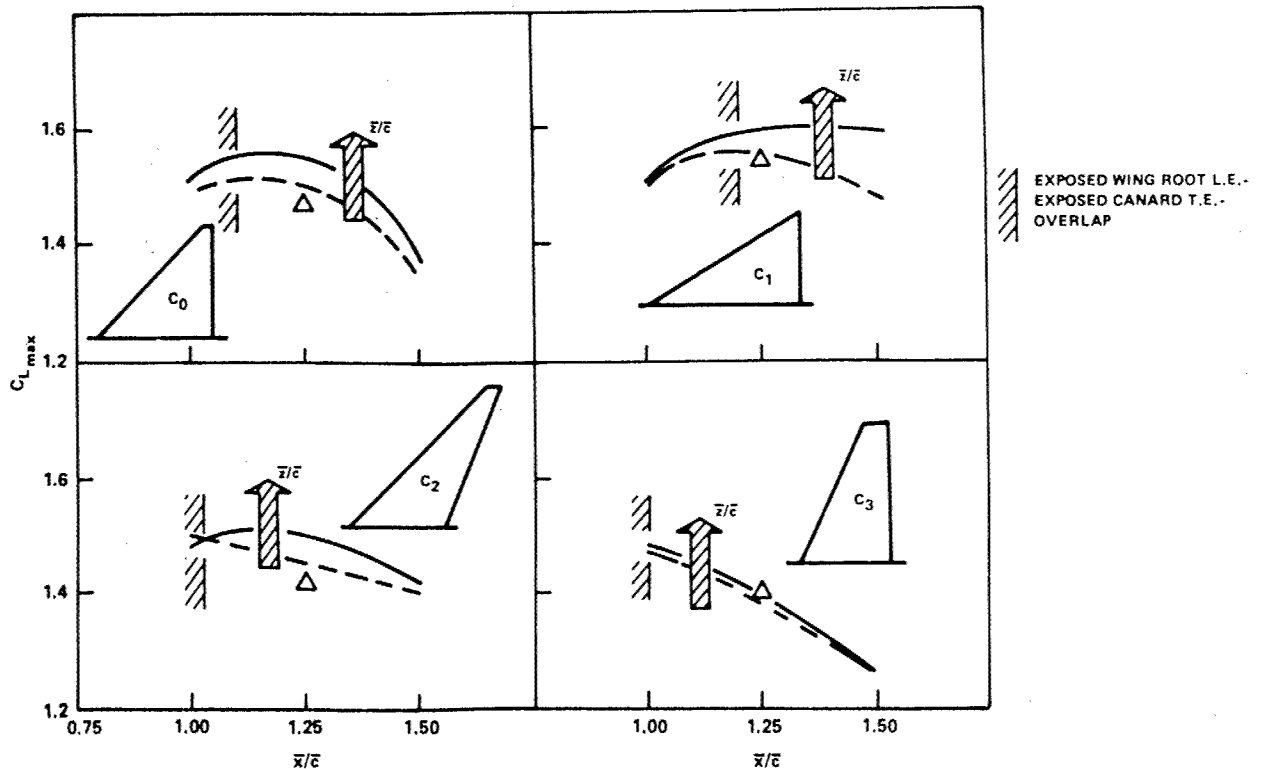
Figure 37 - Maximum Lift Coefficient for Various Canard Shapes

coefficient was developed by the 60-degree delta canard. The normal 45-degree canard had a slightly lower maximum lift coefficient. The high aspect ratio 45-degree canard was lower still, and the 25-degree canard had the lowest maximum lift coefficient. Included on each figure is the $\bar{x}/\bar{c}$ where the canard exposed root trailing edge overlaps the exposed wing root leading edge. Examination of the data relative to the overlap $\bar{x}/\bar{c}$ reveals that maximum lift occurs slightly forward of this value of $\bar{x}/\bar{c}$. Any overlap of the canard causes lift loss.

For all canards other than the delta canard in the high position, there is a significant lift loss if the canard is moved forward. The 60-degree canard C_1 suffers a very slight loss in lift. This behavior is explained by examination of the overlap portion of the canard-wing. Canard overlap for C_0, C_2, and C_3 occurs at an $\bar{x}/\bar{c}$ of approximately 1.0. However, because of the larger root chord of C_1, overlap occurs at an $\bar{x}/\bar{c}$ of approximately 1.2. Thus, the 60-degree canard corresponds, approximately, to P_2

35

for the three other canards. This shift in overlap explains the lack of dropoff for the high canard. The fact that there is a large dropoff in $C_{L_{max}}$ when the 60-degree canard was lowered to the P_4 position is explained by recourse to SAAB TN 60. The 60-degree canard can develop strong leading edge vortices and, if the canard is not properly positioned both longitudinally and vertically, the wing interference can destabilize the canard vortices and cause a lift loss rather than a lift gain. This apparently did occur, because examination of the moment data (presented in Volume 2) reveals a nose down pitching moment, which did not occur for any other position for the 60-degree canard.

The trend in $C_{L_{max}}$ with vertical position follows the trends previously discussed, i.e., lowering the canard reduces $C_{L_{max}}$.

The variation of $(L/D)_{max}$ with canard shape is shown in Figure 38. The order of maximum L/D with canard shape is exactly reversed. The
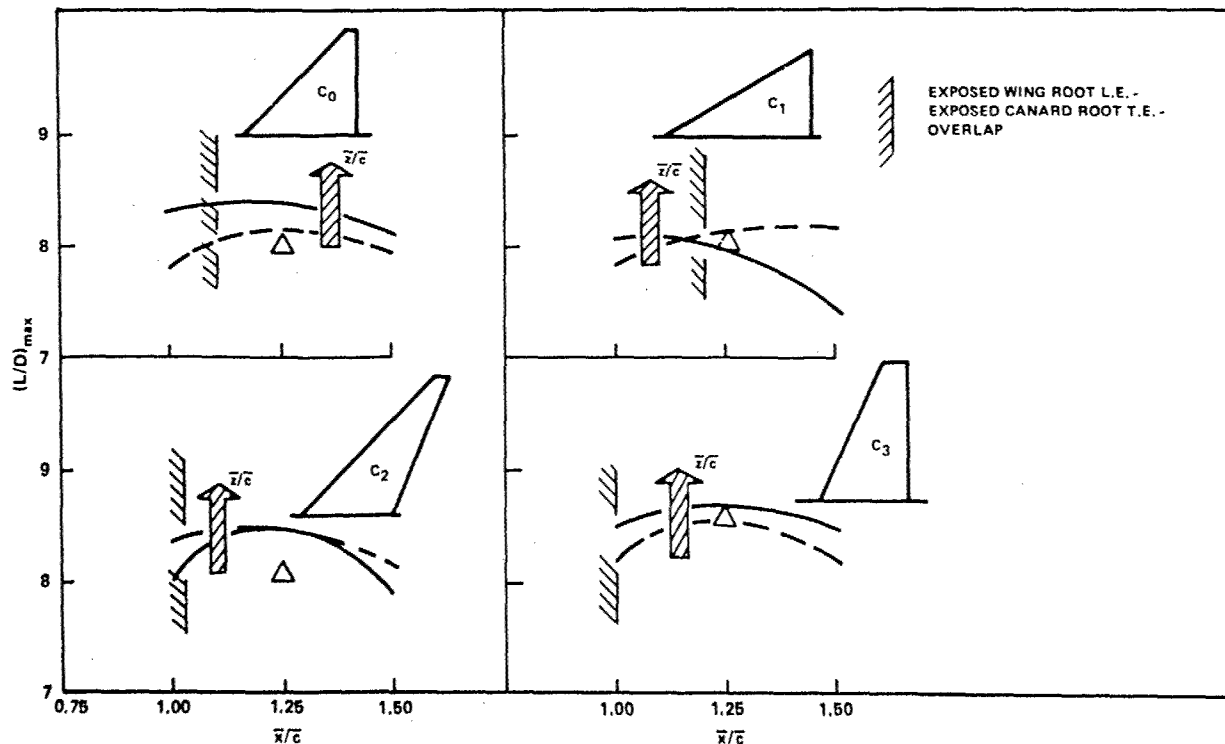

Figure 38 - Maximum Lift-to-Drag Ratio for Various Canard Shapes

25-degree canard C_3 had the highest $(L/D)_{max}$ followed by the 45-degree high aspect ratio canard C_2 and the 45-degree truncated delta canard C_0, with the 60-degree canard having the lowest value of $(L/D)_{max}$. Maximum L/D occurred, in general, between Positions 3 and 2 $(1.0 \leq \bar{x}/\bar{c} \leq 1.25)$. Lowering the canard reduced $(L/D)_{max}$ for all configurations, other than the 60-degree canard.

It is seen that canard shape can have an influence on the desired aircraft characteristics. If high lift is desired, the 60-degree canard is best. If the maximum range, i.e., $(L/D)_{max}$, is desired, the 25-degree high aspect ratio canard performed best.

In order to determine which canard has the best all-round characteristics, the product of $C_{L_{max}}$ and $(L/D)_{max}$ for each canard, made nondimensional by the product for the basic wing body, was determined and is presented in Figure 39. The maximum value of this parameter was achieved by the truncated 45-degree delta canard C_0, followed closely by the 60-degree delta C_1, and then the 45-degree high aspect ratio canard C_2. The 25-degree canard C_3 had the lowest value primarily due to its low maximum lift coefficient. The range between maximum values for the four canards is not great (from 1.36 to 1.42), however; thus any of the canard shapes would perform well if properly located.

MACH NUMBER

The data discussed up to this point were obtained at subsonic speeds. Modern aircraft fly at transonic speeds during many maneuvers. Thus, the effect of the canard at transonic speeds is of great importance. Data are presented in Figure 40 for comparison of the 50-degree wing model both with and without canard at P_3 $(\bar{z}/\bar{c} = 0.2, \bar{x}/\bar{c} = 1.0)$ and at Mach numbers of 0.6, 0.9, and 1.1. Also included in the figure are data for the model with a horizontal tail installed at P_8 $(\bar{z}/\bar{c} = 0.2, \bar{x}/\bar{c} = -1.5)$.

The previous trends noted at subsonic speeds between canard configuration and basic wing-body and/or wing-body-tail occur at transonic speeds. These trends are an increase in lift-curve slope and delay of stall when the canard is compared to either wing-body or wing-body-tail.

37
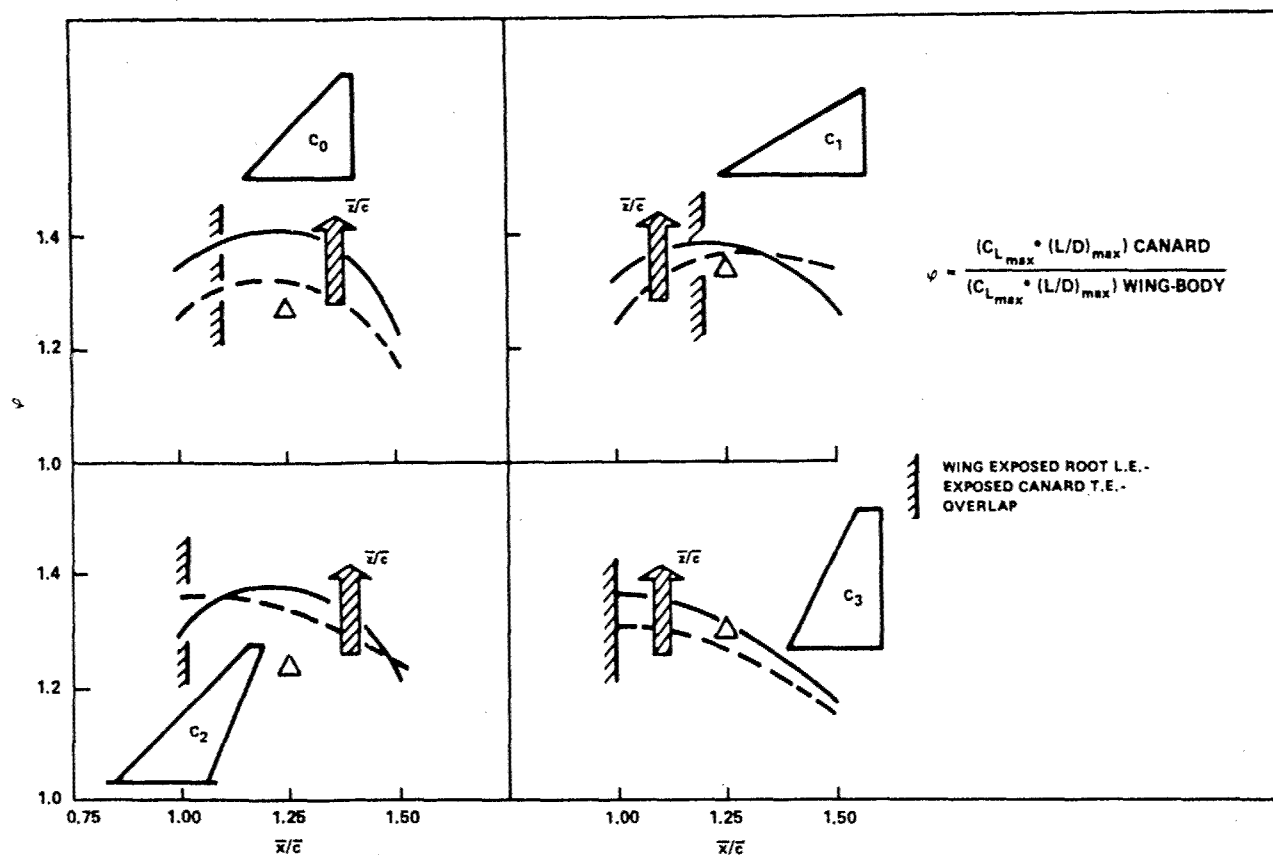
Figure 39 – Product of Maximum Lift-to-Drag Ratio and Maximum
Lift Coefficient for Various Canard Shapes

The increase in lift-curve slope leads to a reduction in drag at lift
coefficients greater than 0.5 for the canard configurations.

Examination of the moment data indicates that the neutral point moves
aft with Mach number increase at about the same rate as the wing-body or
wing-body-tail.

The variation of C_L between canard and wing-body, and canard and hori-
zontal tail, is presented in Figure 41. The plot shows that at low angles
of attack ($\alpha < 12$), the increase in C_L due to the canard is reasonably con-
stant over the Mach number range. At high angles of attack, there is a
decline in the amount of lift increase as the Mach number is increased.
This behavior is due to the improved stall characteristics of the wing-body
and wing-body-tail as Mach number is increased, rather than a deterioration
of the canard characteristics.

Figure 40 – Lift, Pitching Moment, and Drag Coefficient at
Mach Numbers of 0.6, 0.9, and 1.1

Figure 40a – Lift Coefficient

Figure 40b – Pitching Moment Coefficient
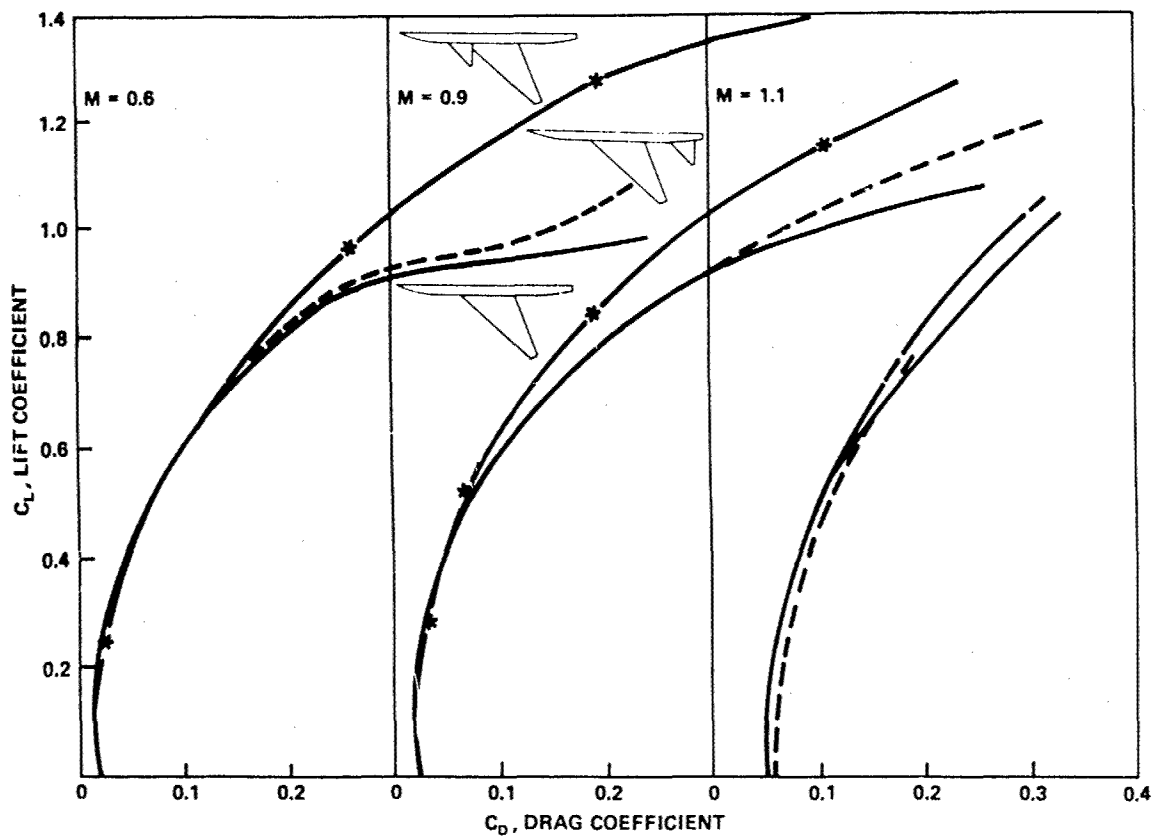
Figure 40c – Drag Coefficient

41
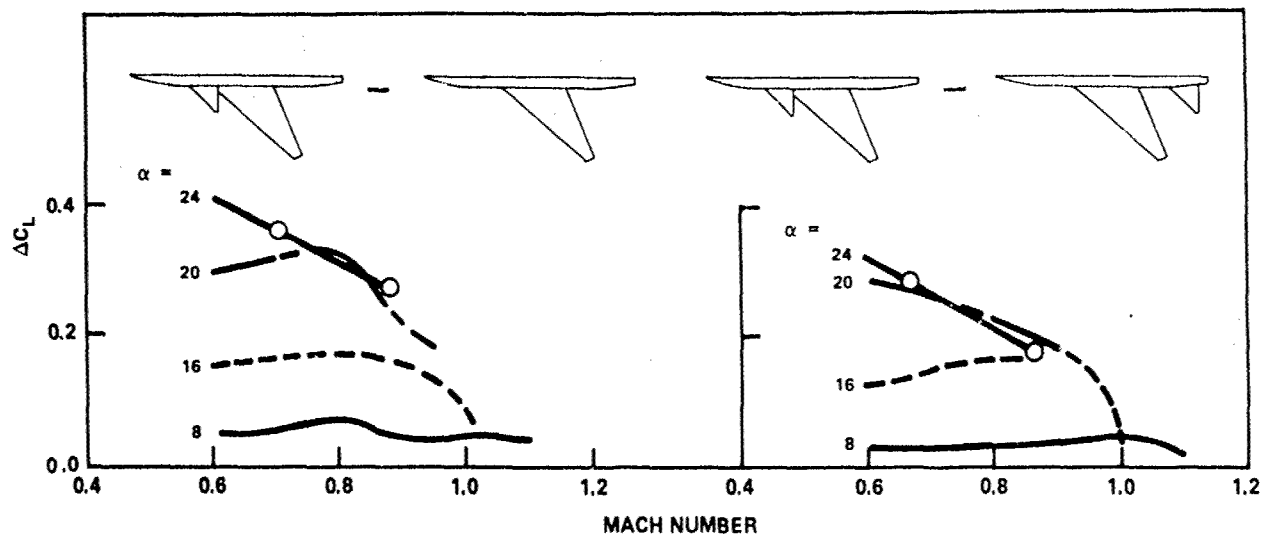
Figure 41 - Variation of Incremental Lift Coefficient due
to Canard with Mach Number

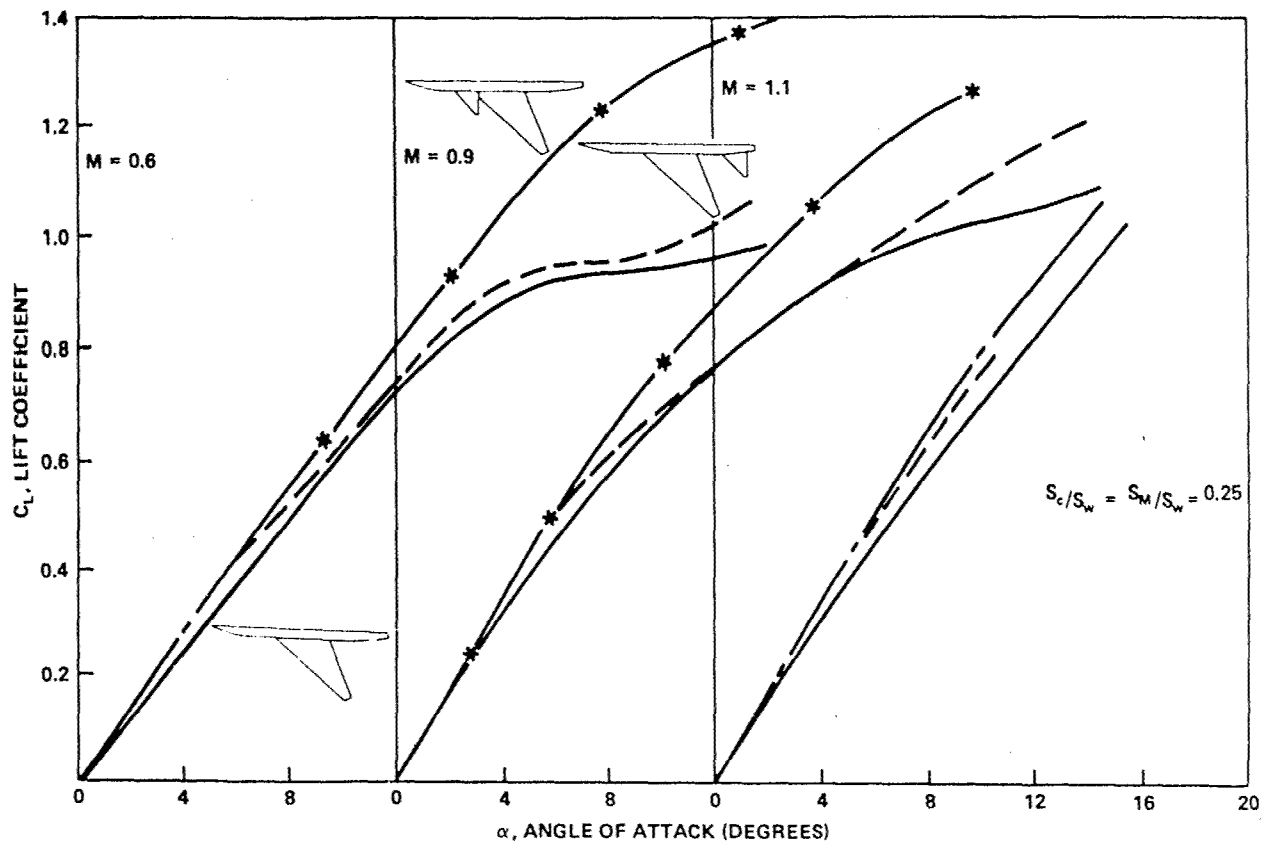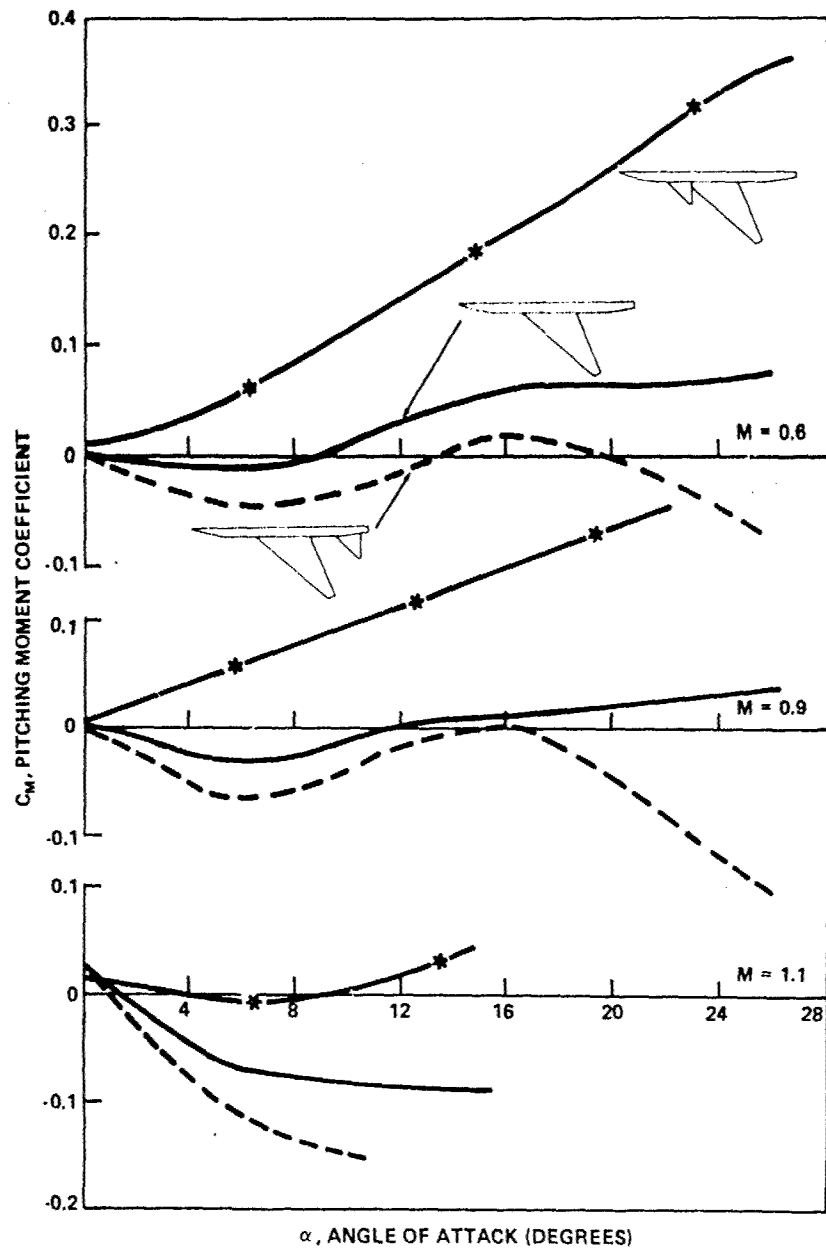The variation of lift-to-drag ratio (L/D) for the canard-wing-body and
wing-body-tail are presented in Figure 42. Again, as with lift data, im-
provements in L/D associated with the canard carry over into the transonic
regime. In general, lift-to-drag ratio at low lift coefficients tended to
fall off with Mach number for the horizontal tail configuration. The
canard configuration tended to have a slight lift-to-drag ratio increase
with increasing Mach number. These trends of L/D with Mach number caused
the peak differential in L/D to occur at Mach numbers between 0.8 and 0.9.
At high lift coefficients, this trend was reversed and the peak dif-
ferential in L/D occurred at M = 0.6.

A comparison of the zero lift drag C_{D_0} values of the canard and hori-
zontal tail configurations is shown in Figure 43. At low Mach numbers
there is little difference in C_{D_0} between canard or horizontal tail. As
Mach number is increased beyond M = 0.8, drag rise is evident for the hori-
zontal tail, whereas, drag rise does not occur for the canard configuration
until approximately M = 0.9. This reduction in wave drag is due primarily
to the area distribution of the basic model. The area distribution for the

42
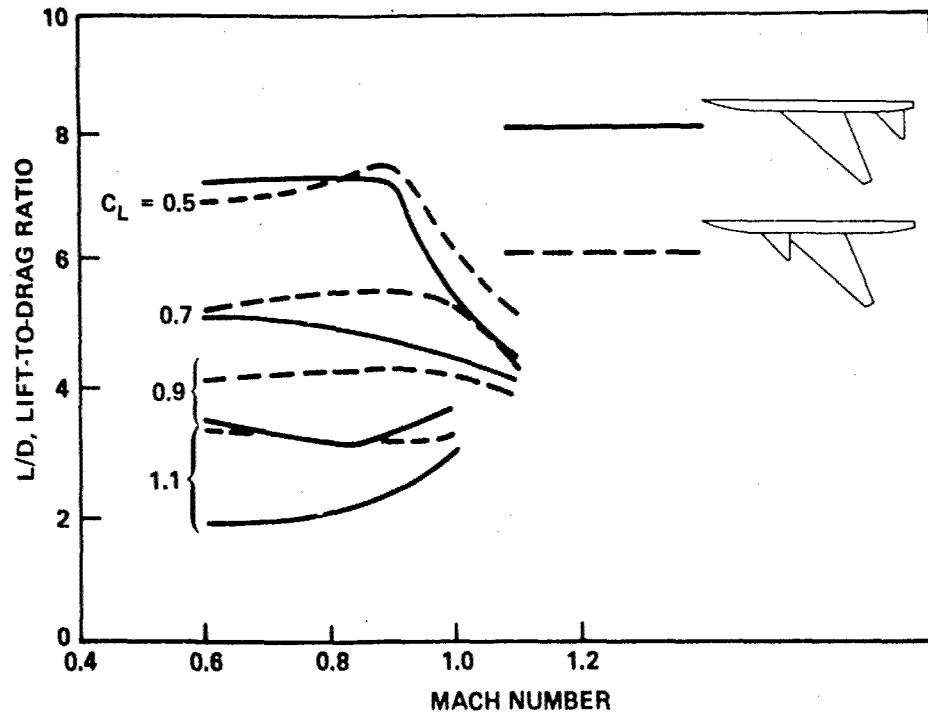
Figure 42 – Variation of Lift-to-Drag Ratio of Canard and
Horizontal Tail with Mach Number
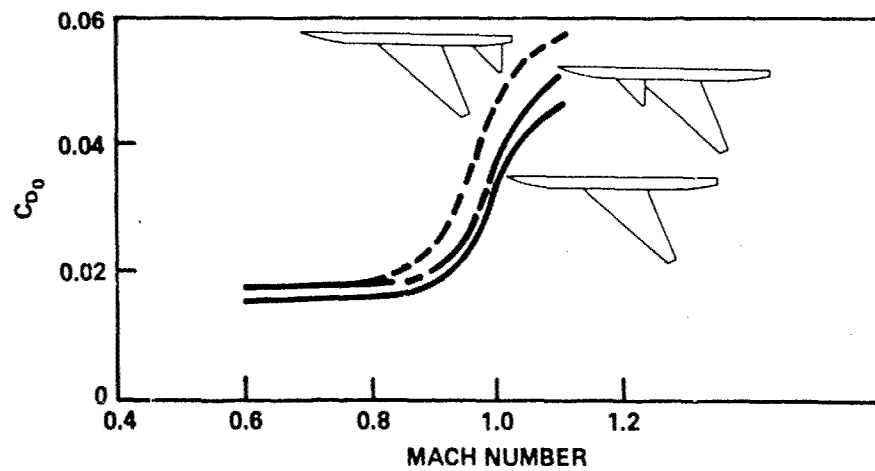
Figure 43 – Variation of Minimum Drag Coefficient
with Mach Number

43

model is shown in Figure 44. As can be seen, the addition of the canard fills in the area distribution between wing and body and fairs into the overall area distribution reasonably well. The horizontal tail, by contrast, adds a distinct bump to the aft body area distribution.
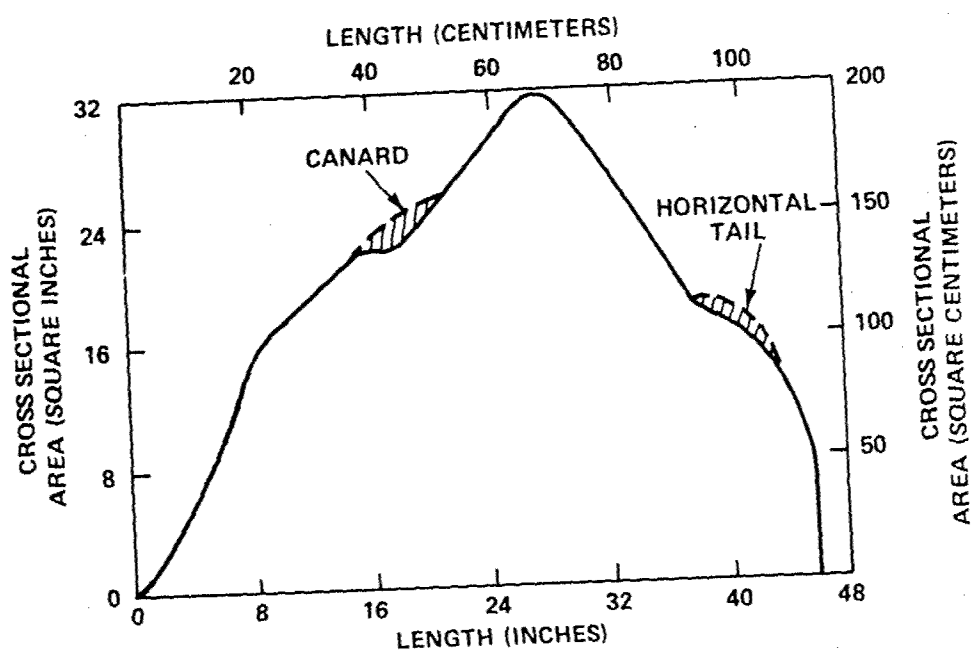
Figure 44 - Area Distribution of 50-Degree Research Model

CONCLUSIONS

The preceeding discussion, although general in nature, has indicated a number of conclusions which can be drawn about the close-coupled canard as applied to low-to-moderate swept wings. These conclusions are as follows:

1. The canard must be within 1.5 wing-chords of the wing quarter chord for favorable interference to occur.

2. Unfavorable interference between wing and canard occurs at low angles of attack for all positions evaluated.

3. The canard must be placed above wing or at least in the plane of the wing for favorable interference at moderate or high angles of attack.

4. The close-coupled canard delays stall of the wing and reduces drag at high lift conditions.

5. An optimum axial and vertical position exists which maximizes both lift and $(L/D)_{max}$. This position is at the point where the canard is slightly forward of the wing-exposed root leading edge. Vertical separation should be between 0.1C and 0.25C.

6. Positive canard deflection causes an increase in drag and decrease in $(L/D)_{max}$. Small negative deflections can cause a slight increase in $(L/D)_{max}$. Neither positive nor negative deflections have a large effect on maximum lift coefficient.

7. Canard shape has an effect on both maximum lift and maximum L/D. Maximum lift requires highly swept canards $\lambda \geq 60$ degrees, where L/D is maximized by low sweep, high aspect ratio canards.

8. The favorable effects and trends noted above hold for Mach numbers up to 1.1.

APPENDIX
MODEL GEOMETRY

The data presented in this report are based on two research models. The models consist of steel wings and a steel central core. Fuselages are wooden fairings surrounding the central core. The canards and horizontal tail are wood and Fiberglass fairings are built up around a steel spar. Attachment of the canards and horizontal tail is provided by steel plates flush with the fuselage. Seven canard and three horizontal tail mounting positions are provided. Each canard can be rotated through a deflection range from -10 to +25 degrees in 5-degree increments. The horizontal tail deflection range is from -25 to +10 degrees. The rotation point for both canards and horizontal tail is 40 percent of the exposed surface root chord. The moment reference point for both research models is $0.27\bar{c}$.

Detailed dimensions of the wings are given in Table 3. Table 4 presents dimensions of the four canards. Dimensions of the horizontal tail are the same as canard C_0. Figure 45 shows the common fuselage shape for both models. Wing-planform geometries are given in Figure 46. Canard geometry is given in Figure 47. Canard and horizontal tail locations are presented in Figure 48. A photograph of the various model components is shown in Figure 49.

TABLE 3 – GEOMETRIC CHARACTERISTICS OF THE WINGS

	W1(λ = 50 degrees)	W2(λ = 25 degrees)
Airfoil Section (NACA)	*	64A008
Projected Area, square inches	304	295
Span, inches	35.50	42.00
Chord, inches		
Root (centerline)	15.38	12.20
Tip	1.90	1.90
Mean Aerodynamic Chord, inches		
Length	10.30	8.30
Spanwise Location from Body Centerline	6.70	7.90
Aspect Ratio	4.15	6.00
Taper Ratio	0.12	0.16
Sweepback Angle, degrees		
Leading Edge	50.0	25.0
Quarter Chord	45.5	20.0
Trailing Edge	23.5	-1.5
Incidence Angle, degrees	0	0
Dihedral Angle, degrees	0	0
Twist Angle, degrees	0	0

*64A008 airfoil swept 25 degrees around 0.27C chord line.

TABLE 4 - GEOMETRIC CHARACTERISTICS OF THE CANARDS

|	C_0	C_1	C_2	C_3
Airfoil Section (NACA)	64A008	64A006	64A008	64A008
Exposed Area, square inches	39.8	39.8	39.8	39.8
Projected Area, square inches	76.0	89.5	76.0	76.0
Exposed Semi-Span, inches	5.74	4.79	7.60	7.60
Total Span, inches	16.28	14.38	20.00	20.00
Chord, inches				
Root (centerline)	8.73	12.45	6.70	6.12
Root (exposed)	6.33	8.30	5.31	5.00
Tip	0.59	0	0.90	1.48
Aspect Ratio	3.50	2.31	5.26	5.26
Taper Ratio	0.70	0	0.13	0.24
Sweepback Angle, degrees				
Leading Edge	45	60	45	25
Trailing Edge	0	0	22.8	0
Dihedral Angle, degrees	0	0	0	0

49

A ←
A ←
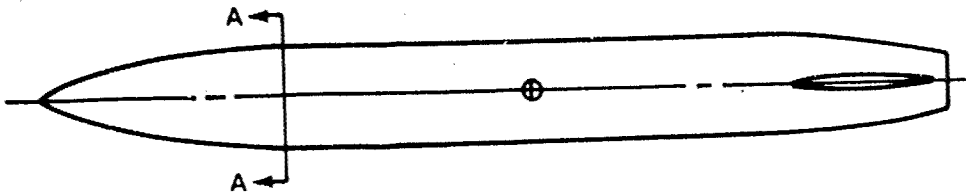
Figure 45a – Top View

SECTION A-A

ALL DIMENSIONS ARE IN INCHES (CENTIMETERS)

WIDTH = 4.75 (12.06); HEIGHT = 4.15 (10.54)
UPPER CORNER RADIUS = 1.00 (2.54)
LOWER CORNER RADIUS = 0.25 (0.64)

25.12
(63.80)

45.62
(115.87)
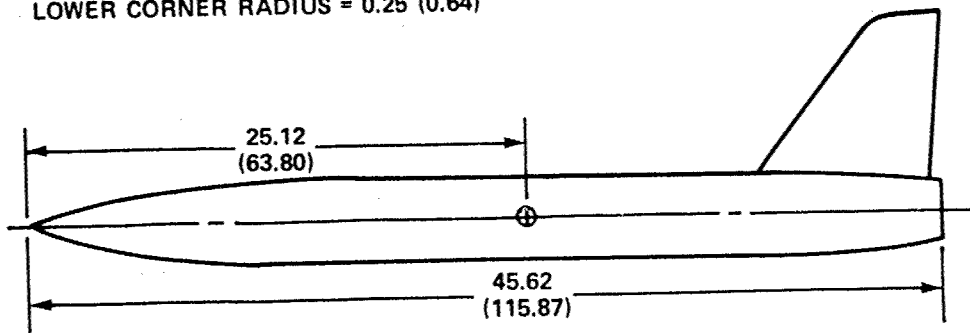
Figure 45b – Side View

Figure 45 – Research Aircraft Fuselage
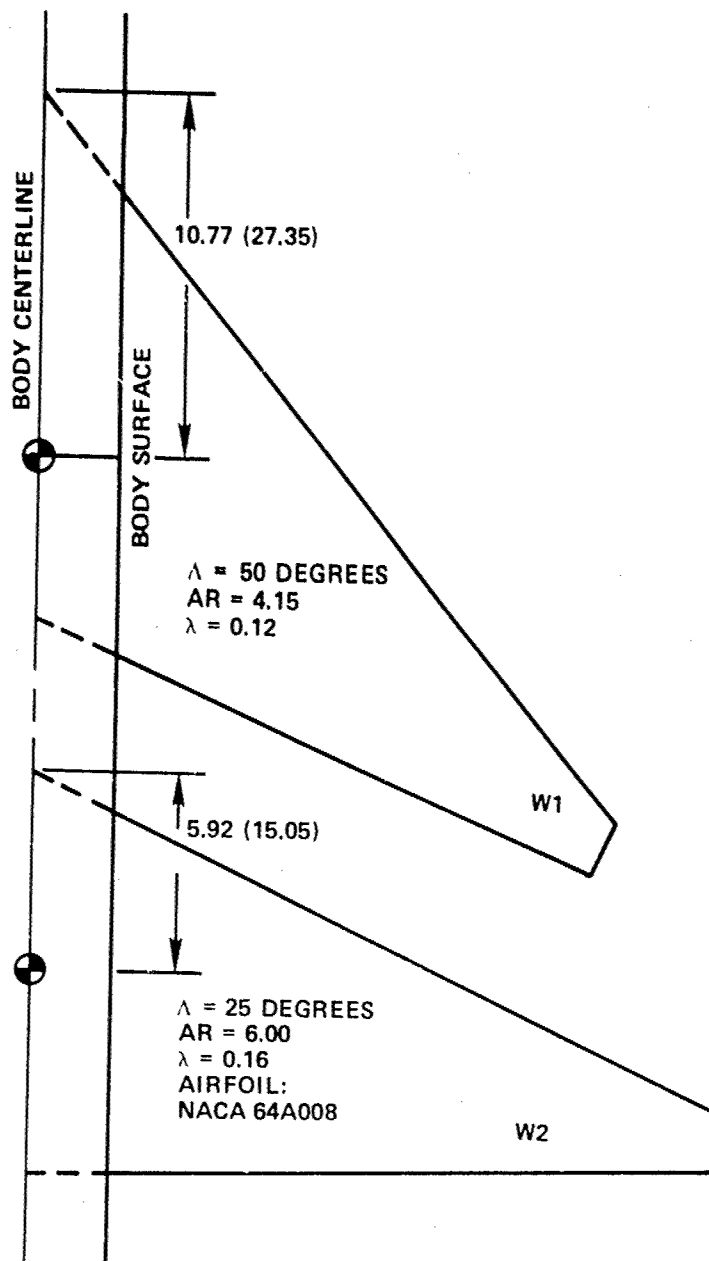
Figure 46 - Planform View of the Wings

Λ = 45 DEGREES
AR = 3.50
λ = 0.07
AIRFOIL:
NACA 64A008

c_0

Λ = 45 DEGREES
AR = 5.26
λ = 0.13
AIRFOIL:
NACA 64A008

c_2

BODY CENTERLINE

BODY SURFACE

Λ = 25 DEGREES
AR = 5.26
λ = 0.24
AIRFOIL:
NACA 64A008

Λ = 60 DEGREES
AR = 2.31
λ = 0
AIRFOIL:
NACA 64A006

c_3

c_1

Figure 47 – Planform View of the Canards

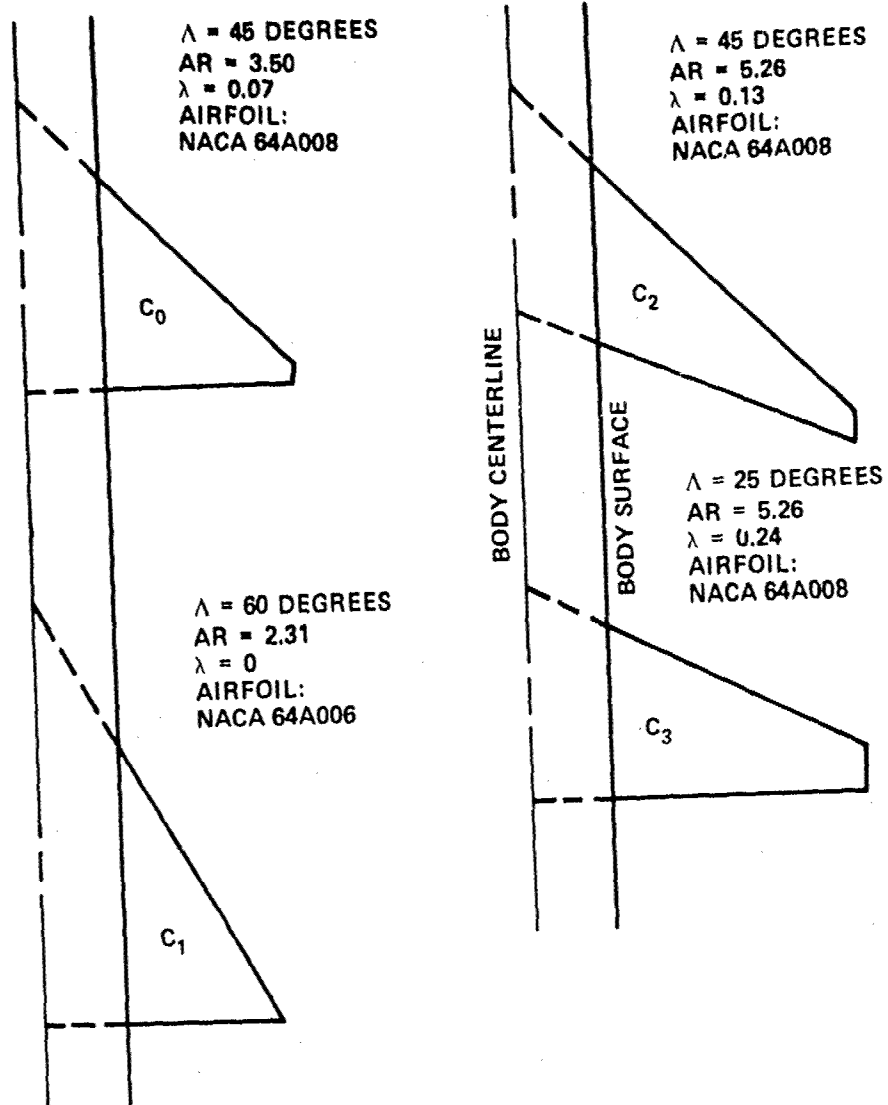NOTE: ALL DIMENSIONS ARE IN INCHES (CENTIMETERS)
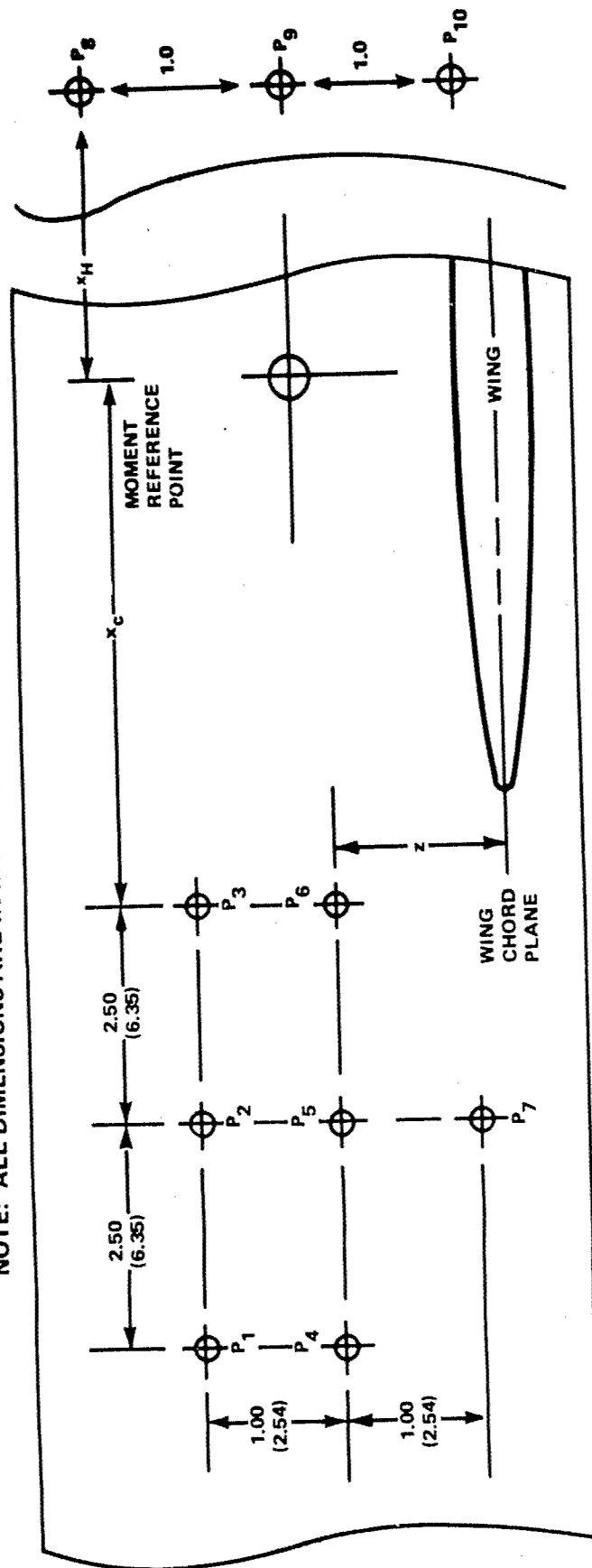
W1 ($\Lambda = 50$ DEGREES): $x_c = 10.00$ (25.40); $z = 1.40$ (3.56), $x_H = 15.00$ (38.10)

W2 ($\Lambda = 25$ DEGREES): $x_c = 7.18$ (18.24); $z = 1.14$ (2.90)

Figure 48 – Canard Pivot Locations

53

Figure 49 - Wind-Tunnel Model Components

REFERENCE

1. Behrbohm, H., "Basic Low Speed Aerodynamics of the Short-Coupled Canard Configuration of Small Aspect Ratio," SAAB TN 60 (Jul 1965).

INITIAL DISTRIBUTION

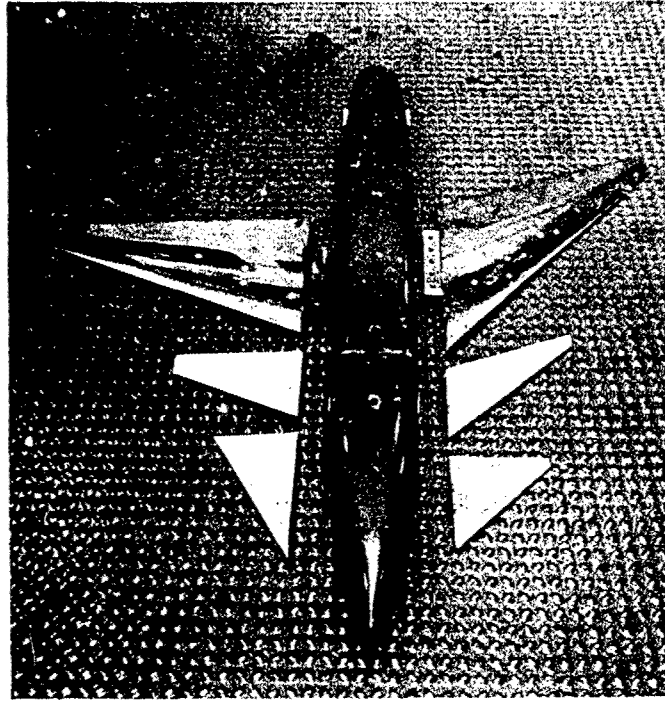| Copies			Copies	
1	CHONR/Dr. R. Whitehead		1	North American Rockwell/ Los Angeles/Lib
3	NADC			
	1	Terry Miller (V/STOL Project Office)	1	Northrop Corporation/Irv Waller
	1	Bill Becker		
	1	Carman Mazza	1	LTV/H. Diggers
2	NAVAIR			
	1	AIR-03		CENTER DISTRIBUTION
	1	AIR-530		

CENTER DISTRIBUTION

Copies	Code	Name
10	5214.1	Reports Distribution
1	522.1	Library (C)
1	522.2	Library (A)
2	522.3	Aerodynamics Library

Copies	
12	DDC
1	AFFDL/Capt Bill Sotomayer
1	NASA HQ/Scientific Tech Info Branch
1	NASA Ames/Preston Nelms
3	NASA Langley
	1 Joe Chambers
	1 Blair Gloss
	1 Bill Henderson
1	Boeing Aerospace Company/H. Yoshihara
1	General Dynamics/Fort Worth/ C.E. Kuchar
1	Grumman Aerospace Corporation/ Nick Dannerhoffer
1	Lockheed-California/Andy Byrnes
2	McDonnell Douglas Corp/ St. Louis
	1 Jim Sinnett/MCAIR
	1 Jim Hess/MCAIR
1	North American Rockwell/ Columbus/Lib

DTNSRDC ISSUES THREE TYPES OF REPORTS

1. DTNSRDC REPORTS, A FORMAL SERIES, CONTAIN INFORMATION OF PERMANENT TECH
NICAL VALUE. THEY CARRY A CONSECUTIVE NUMERICAL IDENTIFICATION REGARDLESS OF
THEIR CLASSIFICATION OR THE ORIGINATING DEPARTMENT.

2. DEPARTMENTAL REPORTS, A SEMIFORMAL SERIES, CONTAIN INFORMATION OF A PRELIM-
INARY, TEMPORARY, OR PROPRIETARY NATURE OR OF LIMITED INTEREST OR SIGNIFICANCE.
THEY CARRY A DEPARTMENTAL ALPHANUMERICAL IDENTIFICATION.

3. TECHNICAL MEMORANDA, AN INFORMAL SERIES, CONTAIN TECHNICAL DOCUMENTATION
OF LIMITED USE AND INTEREST. THEY ARE PRIMARILY WORKING PAPERS INTENDED FOR IN-
TERNAL USE. THEY CARRY AN IDENTIFYING NUMBER WHICH INDICATES THEIR TYPE AND THE
NUMERICAL CODE OF THE ORIGINATING DEPARTMENT. ANY DISTRIBUTION OUTSIDE DTNSRDC
MUST BE APPROVED BY THE HEAD OF THE ORIGINATING DEPARTMENT ON A CASE-BY-CASE
BASIS.